Republic of Iraq
Ministry of Higher Education
& Scientific Research
University of Baghdad
College of Education for pure Science Ibn Al-Haitham

Theoretical study to design plasma focus machine and investigate various parameters that affect its emitted neutron yield

A Thesis
Submitted to the Council of College of Education
Ibn Al-Haitham University of Baghdad
in Partial Fulfillment of the Requirements for
the Degree of Master in
Science physics

By

Rana Issa Bk-murd Mahmud

Supervisor

Assist. Prof .Dr. Mustafa Kamel Jassim
Assist. Prof .Dr. Raad Hameed Majeed

2014 A.D. **1435 A.H.**

بسم الله الرحمن الرحيم

(يـــَا مَعشَـــرَ الجـــِنّ وَالإنِـــس إنِ اســـتَطَعتُم أن تَنفُذُواْ مِن أقطَـارِ السَّماواتِ وَالأرضِ فأنفُذُواْ لا تَنفُذُونَ إلا بِسُلطَانٍ)

صدق الله العظيم

{ الرحمَّـنْ الآية 33}

الأهــداء

الى من بنوره اهتديت وعليه توكلت

... الرحمن الرحيم....

الى من بوجوده أنيرت السماوات والأرض

.... محمد المصطفى (ص) ....

الى من أزهارجهده أثمرت ذهباً.... والدي العزيز ....

الى صحوة فؤادي وقرة عيني.... والدتي العزيزة ....

الى أساس سندي في الحياة....أخوتي وأخواتي الأعزاء ....

الى بحر العلم والمعرفة.... أساتذتي ....

الى كل من تعلمنا على أيديهم وكللوا جهودنا بالنجاح نهدي هذا الجهد المتواضع

.... اعترافاً وشكراً وتقديراً ....

رنـــا

Acknowledgements

First and foremost I would like to express my deep gratitude and thanks to God "**Allah**". I can't learn and complete my research without God's help**.**

I would like to take this opportunity to express my deep appreciation and thanks for my supervisors: Dr. Mustafa Kamel Jassim and Dr. Raad Hameed Majeed for their constant support and encouragement through research stage.

I wish also to thank the head of Physics Department, and all the staff of department in the College of Education Ibn Al-Haitham in the University of Baghdad, for their support and giving me this opportunity to continue my M.Sc. study.

Finally, I want to thank my family: My parents, who always supported me and encouraged me in pursuing a scientific journey and too, of course, of my brothers and all beloveds for me.

Rana Issa Bk-Murd

Supervisor's Certification

We certify that this thesis was prepared under our supervision at University of Baghdad / College of Education Ibn- Al – Haitham / Department of Physics in partial fulfillment of the requirements for the degree of **Master of Science in Physics**.

Signature:

Assist. Prof. Dr. Mustafa Kamel Jassim
Title: Supervisor
Date: / / 2014

Assist. Prof. Dr. Raad Hameed Majeed
Title: Supervisor
Date: / / 2014

In view of the available recommendation, we forward this thesis for debate by the examining committee.

Signature:

Name: Dr. Mohamed Abd Al-Nabee

Title: (Assist Professor)

"Chairman of Physics Department"

Date: / / 2014

Committee Certification

We certify that we have read this thesis, entitled " **Theoretical study to design plasma focus machine and investigate various parameters that affect its emitted neutron yield "** and as examining committee, examined the student **Rana Issa bk-Murd** on its contents, and that in our opinion it is adequate for the partial fulfillment of the requirements for the degree of master of science in physics. Therefore recommended her for this degree.

Signature: **Name: Hydar A. R Salih** **Date: / / 2015** **(chairman)**	**Signature:** **Name: Dr. Bushra Joudah Hussein** **Date: / / 2015** **(Member)**
Signature: **Name: Ass. Prof. Dr. Intesar H. Hashim** **Date: / / 2015** **(Member)**	**Signature:** **Name: Dr Mustafa K Jassim** **Dr.Raad .H .Majeed** **Date: / / 2015** **(Member and supervisor)**

Approved by the University Committee of postgraduate studies.

Signature:

Name: Assist .prof . Dr. Khalid Fahad Ali

Dean of the Ibn –Al-Haitham College of Education, University of Baghdad

Date: / /2015

Abstract

In this work the design of a dense plasma focus based on (Lee) model theoretically achieved. The model contains of mathematical treatments of DPF system including description of engineering configuration of system elements such as electrodes and elements of the electrical circle, which includes capacitance, inductance and resistance (RLC). to introduce new design based on Lee program. After the necessary calculations has been achieved, the results of design are introduced in the program to notice theoretically the extent of interoperability of the machine throughout the study of various parameters provided by the program and thus to identify the operating conditions and the factors influencing it.

Deuterium (D) was chosen as working gas in this machine to obtain high neutron output (1.66×10^8 neutron per shot) for a fusion nuclear reaction. The study and testing the system at two pressures (3 Torr and 4 Torr) are achieved through various parameters provided by the program and the results are compared and discussed graphically. In addition, the designed system has been compared to a standard system that has structure similarities. A theoretical NX2 dense plasma focus system, which was built mainly to use with noble gases to obtain X-ray, is chosen with deuterium gas to obtain neutron output for the sake of comparison where most of the operating parameters of both the designed and the standard are studied graphically and the behavior parameters of both systems such as (the tube total current, tube voltage, axial speed, axial position trajectory, radial inward shock trajectory, pinch elongation trajectory, pinch elongation speed, radial

reflected shock trajectory and speed, plasma temperature with time). The losses generated from both systems such as Joule Heat, Bremsstrahlung energy and recombination energy and line radiation energy with time is calculated and represented graphically.

Finally it is found that the designed system provides greater neutron yield (1.66 × 10^8 neutron per shot) higher than the standard system (5.15 × 10^7 neutron per shot) . The designed system behaves like the general systems of dense plasma focus. The difference in the behavior of the designed and standard system comes from the geometry different of the both systems in terms of engineering electrodes and the values different of electric elements of RCL circuit. The theoretical designed system in this research could be a project to build a machine of dense plasma focus required for nuclear fusion reaction due to its advantage of yielding high neutron.

List of Symbols

Symbol	*Description*
n	Particle density in plasma
T	Plasma temperature
B	Magnetic field
$f(u)$	Velocity distribution function
u	Total velocity
m	Mass of the particle
k	Boltzmann's constant
λ_D	Debye length
T_e	Electron temperature
n_e	Electron number density
ε_0	Permittivity of free space
e	Electron charge
N_D	*N*umber of electrons in a Debye sphere
v_e	Electron thermal velocity
v_i	Ion’s thermal velocity
m_e	Electron mass
m_i	Ion’s mass
ω_{pe}	Electron plasma frequency
ω_{cs}	Cyclotron frequency
λ_{mfp}	Mean free path for collisions
τ	Mean time between collisions
u_e	Electrons velocity
ν_c	Collision frequency

Symbol	***Description***
n_a	Number density of the neutral gas
$\bar{u}$	Thermal speed of charged particles
σ	Collision cross-section
Λ	Plasma parameter
ω_p	Langmuir frequency
τ_E	Confinement time
m_p	Mass of the plasma sheath
ρ_0	Gas density
a	Anode radius
b	Cathode radius
z_a	Axial position of the current sheath
f_m	Fraction of mass swept down the axial direction
B_θ	Induced magnetic field
F	Magnetic force on current sheath
I_p	Current flown through the plasma
μ	Permeability of space
f_c	Fraction of current flowing in the piston
I	Discharge Current
V_0	Initial charge voltage
C_0	Energy storage capacitance
R_0	Stray circuit resistance
R_p	Resistance of the plasma focus tube
L_p	Inductance of the plasma focus tube
Z_0	Surge impedance
t_0	Time of the L C circuit
I_0	Current of the L – C circuit

Symbol	***Description***
t_a	Characteristic axial transit time
β	Ratio of load to source inductance
δ	Ratio of circuit stray resistance to surge impedance
P_s	Shock wave pressure
v_s	Shock front speed
$\mathrm{P_m}$	Magnetic pressure
r_p	Radial piston position
r_s	Radial shock front position
f_{mr}	Modified f_m value in the radial phase
γ	Specific heat ratio of the operating gas
L_f	Inductance of the radially imploding and elongating plasma pinch
Q_j	Resistive heating
Q_B	Bremsstrahlung loss
Q_L	Line loss or Energy line radiation
N_i	Number density
Z_e	Effective charge number
Z_n	Atomic number of gas
r_{pinch}	Pinch radius
z_{pinch}	Pinch length
Q_{rec}	Recombination loss
ξ_f	Length of the focus column
v_m	Macroscopic speed of the sheath during rundown
$I_{0,\mathrm{peak}}$	Maximum ideal current
l	Total length of the electrodes
E	Bank energy

Contents

Chapter Three

Lee Code

Chapter Four

Results and Discussion

CHAPTER

ONE

Introduction

Introduction

1.1: Plasma

Plasmas constitute more than 99.9% of the mass of the known universe, being the principal ingredient of stars. However, on earth they are less common; they can be seen as lightning, the Aurora Borealis. Plasmas exist naturally or are man-made. The flame from a fire is an example of naturally existing plasma. Examples of man-made plasmas are various gas and fluorescent lamps, DC and RF deposition and sputtering systems, and a welder's arc discharge. They are often referred to as the fourth state of matter, and contain a multitude of species including electrons, neutrals, ions and electromagnetic radiation. They are quasi – neutral, possessing roughly equal numbers of negative and positively charged species. The plasma was first used by Irving Langmuir in 1928 to describe the ionized gas in an electric discharge [1].

When a solid (the first state of matter) is heated, the particles in it get sufficient energy to loosen their structure and thus melt to form a liquid (the second state of matter). After obtaining sufficient energy, the particles in a liquid escape from it and vaporize to gas (the third state of matter). Subsequently, when a significant amount of energy is applied to the gas through mechanisms such as an electric discharge, the electrons that escape from atoms or molecules not only allow ions to move more freely but also produce more electrons and ions via collisions after accelerating rapidly in an electric field. Eventually, the higher number of electrons and ions change the electrical property of the gas, which thus becomes ionized gas or plasma [2].

In the plasmatic state the electrons are completely separate from the atoms and therefore have entire freedom of movement. If atoms or molecules have lost one or more electrons they carry positive charge outwardly, in this case they become positive ions. "Plasma" is therefore considered as gas showing collective behavior (because the electrostatic force is a long range force and every charged particle interacts with many of its neighbors.) and consisting of particles which carry positive and negative charges – in the extent that the overall charge comes to zero. Plasma is electrically neutral to the outside, if the number of

positive and negative charges equals in a sufficiently large volume and for a sufficiently long interval of time. This balance is referred to as "quasi neutrality" [3] ("quasi" because the small deviations from exact neutrality have important dynamical consequences for certain types of plasma mode).

In some cases it is suggested that the plasma is not the fourth state of matter because of the large size of the temperature range within which the transition from the 'neutral' to 'completely ionized gas' takes place. However, this objection cannot be regarded as important because the criterion of the plasma state does not include the degree of ionization [4].

1.2: Characteristic Plasma Parameters

Since the plasma state occupies an extremely wide range of densities, temperatures and magnetic field strengths it is convenient to define several characteristic plasma parameters. Three fundamental parameters characterize a plasma [5]:

1. The particle density n (measured in particles per cubic meter),
2. The temperature T of each species (usually measured in eV, where $1\ \mathrm{eV} = 11{,}605\ \mathrm{K}$),
3. The steady state magnetic field B (measured in Tesla).

1.2.1: Plasma Number Density and Temperature

The plasma, as defined, consists of charged particles, namely electrons and ions. A gas is characterized by the number of particles per unit volume, which we call the number density n (m^{-3}). The motion of the particles (in thermodynamic equilibrium) is determined by the temperature T of the gas. in the thermal equilibrium, all the components of the system have the same temperature or average kinetic energy.

At thermal equilibrium the velocity distribution function becomes a Maxwellian distribution and which is given by [6]:

$$f(u) = Aexp(-\frac{1}{2}mu^2/k_BT) \qquad (1\text{-}1)$$

The constant *A* is found *b*y imposing $n = \int_{-\infty}^{+\infty} f(u)du$

where $A = n(\frac{m}{2\pi k_{BT}})^{\frac{1}{2}}$, $f(u)$ is the velocity distribution function $[m^{-6} - s^3]$, u is the total velocity , m is the mass of the particle , k is the Boltzmann's constant $(k_B = 1.381 \times 10^{-23} Jk^{-1})$, T is the plasma temperature .

1.3: Debye Length

A fundamental characteristic of the behavior of a plasma is its ability to shield out electric potential that applied to it.
Suppose we put an electric field inside a plasma by inserting two charged balls connected to a battery (Figure 1-1).

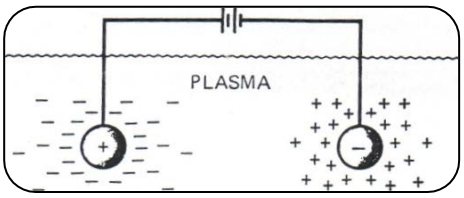

Figure 1-1: Debye shielding [7].

The balls would attract particles of the opposite charge, and almost immediately a cloud of ions would surround the negative ball and a cloud of electrons would surround the positive ball. (We assume that a layer of dielectric keeps the plasma from actually recombining on the surface, or that the battery is large enough to maintain the potential in spite of this.) If the plasma were cold and there were no thermal motions, there would be just as many charges cloud as in the ball; the shielding would be perfect, and no electric field would be present in the body of the plasma outside of the clouds. On the other hand, if the temperature is finite, those particles that are at the edge of the cloud, where the electric field is weak, have enough thermal energy to escape from the electrostatic potential well. The "edge" of the cloud then occurs at the radius where the potential energy is approximately equal to the thermal energy KT of the particles [8].

The Debye length can be expressed simply as

$$\lambda_D = \sqrt{\frac{\varepsilon_0 k T_e}{n_e e^2}} \qquad (1\text{-}2)$$

where T_e is the electron temperature, n_e is the electron number density, ε_0 is the permittivity of free space ($\varepsilon_0 = 8.854 \times 10^{-12} m^{-1}$), and e is the electron charge.

This provides condition to determine if we have a plasma or not.

(i) The system must be large enough $L \gg \lambda_D$.
For a length L much smaller than λ_D, the plasma should exhibit quasi neutral behavior, i.e. the net charge density is zero.

(ii) There must be enough electrons to produce shielding $N_D \ggg 1$, where N_D is the number of electrons in a Debye sphere. The number of particles in a Debye sphere is N_D. This condition makes sure that the collisional influence is not too large in the plasma, and that the dynamics is dominated by collective forces. In case this condition is not fulfilled, which behave quite differently from normal plasmas.

The number of electrons N_D in a Debye sphere is [9]:

$$N_D = \frac{4}{3}\pi \lambda_D^3 n_e \qquad (1\text{-}3)$$

where N_D is usually large for hot or rarefied gases and small for dense or cool gases.

1.4: Plasma Sheaths

Plasmas, which are quasi-neutral ($n_e = n_i$), are joined to wall surfaces across thin positively charged layers called sheaths.

Formation of the positively charged sheaths is due to the fact that electrons are much faster than ions, and the electron thermal velocity ($v_e = \sqrt{kT_e/m_e}$) is about 1000 times faster than the ion's thermal velocity ($v_i = \sqrt{kT_i/m_i}$). The fast electrons are able to stick to the wall surface, leaving the area near the walls for positively charged ions alone , where v_e is the thermal velocity, v_i is the ions velocity, m_e is the electron mass and m_i is the ion mass [10].

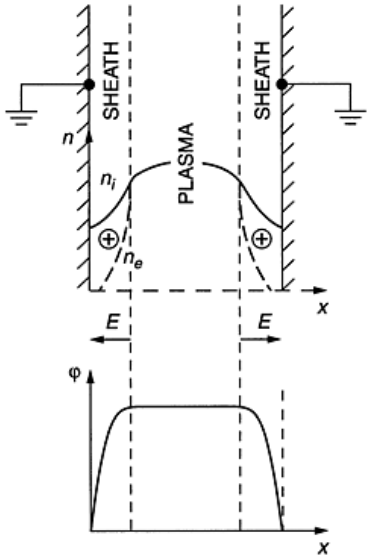

Figure 1.2: Plasma and sheaths [11].

Consider a plasma of $n_e = n_i$ initially confined between two grounded ($\varphi = 0$) absorbing walls. Because the net charge density is zero, the electric potential φ and the electric field E_x is zero everywhere. Hence, the fast-moving electrons are not confined and will rapidly be lost to the walls. On a very short timescale, however, some electrons near the walls are lost, leading to the situation shown in Figure 1.2. Thin positive ion sheaths form near each wall in which $n_e \gg n_i$. The net positive ρ within the sheaths leads to a potential profile φ (x) that is positive within the plasma and falls sharply to zero near both walls. This acts as a confining potential "valley" for electrons and a "hill" for ions because the electric fields within the sheaths point from the plasma to the wall. Thus the force $-eE_x$ acting on electrons is directed into the plasma; this reflects electrons traveling toward the walls back into the plasma. Conversely, ions from the plasma that enter the sheaths are accelerated into the walls. If the plasma potential (with respect to the walls) is V_p, then we expect that $V_p \sim$ a few T_e in order to confine most of the electrons. The energy of ions bombarding the walls is then $\varepsilon_0 \sim$ a few T_e [12].

1.5: Plasma Frequency

The plasma frequency, is the most fundamental time-scale in plasma physics. Clearly, there is a different plasma frequency for each

species. However, the relatively fast electron frequency is, by far, the most important, and references to "the plasma frequency" in text-books invariably mean the electron plasma frequency [13].

This frequency come to because the collision. The weakly ionized gas in a jet exhaust, for example, does not qualify as a plasma because the charged particles collide so frequently with neutral atoms that their motion is controlled by ordinary hydrodynamic forces rather than by electromagnetic forces. If ω is the frequency of typical plasma oscillations and τ is the mean time between collisions with neutral atoms, we require $\omega\tau > 1$ for the gas to behave like a plasma rather than a neutral gas.

$$\omega_{pe} = \sqrt{\frac{n_e e^2}{\varepsilon_0 m_e}} \qquad (1\text{-}4)$$

where ω_{pe} is the electron plasma frequency and m_e is the electron mass. The three conditions a plasma must satisfy are therefore [14]:

1. $\lambda_D \ll L$
2. $N_D >>> 1$
3. $\omega\tau > 1$

1.6: Cyclotron Frequency

A charged particle of mass m_s and charge q_s will exhibit circular motion in a plane normal to an external, uniform magnetic field, B, with a characteristic frequency called the cyclotron frequency, given by

$$\omega_{cs} = 2\pi f_{cs} = \frac{q_s B}{m_s} \qquad (1\text{-}5)$$

The cyclotron frequency is used as a way to measure the plasma parameters because the plasma emits radiation at the cyclotron

frequency and its harmonics. This radiation can be detected in a variety of ways depending on its intensity and duration [15].

1.7: Collision

Collisions between charged particles in a plasma differ fundamentally from those between molecules in a neutral gas because of the long range of the coulomb force. Collisions of charged particles in a plasma are of two types: The first one occurs between charged particles and neutral particles, while the second one occurs between charged particles. In the case collision between charged and neutral particles the interaction force has a very short range and the scattering process is similar to the scattering produced by hard spheres. This collision frequency is important in the partially ionized plasma. The non-equilibrium plasma pinch may be considered as a partially ionized plasma in the early evolution of the pinch. In the case collisions between charged particles Collisions between charged particles are a consequence of the long range Coulomb force effect. The long range Coulomb force effects become significant when the plasma is fully ionized. That is, small angle collision effects (long range Coulomb effects) are typically dominant in a plasma compared to large collisions. During the stagnation time of the pinch, it is desired to thermally ionize the trapped particles so to approach the fully ionized state [16].

For example, can be expressed in terms of the equivalent cross section σ that an atom would have if it were ionized by all electrons striking within this cross sectional area.

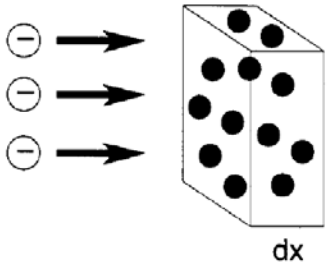

Figure 1.3: Electrons incident on a thin slab of thickness dx containing neutral atoms of density n [17].

In this Figure 1.3 electrons are incident upon a thin slab of thickness dx containing $n,$ neutral atoms per unit volume. The atoms are imagined to be opaque spheres of cross sectional area σ The number of atoms per unit area of the slab is $n_n dx$, and the fraction of the slab blocked by atoms is $n_n \sigma dx$ so that the change of flux Γ with distance x is given by

$$\frac{d\Gamma}{dx} = -n\sigma\Gamma \tag{1-6}$$

which has the solution

$$\Gamma = \Gamma_0 \exp(-n_n \sigma x) = \Gamma_0 \exp\left(-x/\lambda_{mfp}\right) \tag{1-7}$$

where

$$\lambda_{mfp} = \frac{1}{n_n \sigma} \tag{1-8}$$

The quantity λ_{mfp} is called the mean free path for collisions. In a distance λ_{mfp}, the flux would be decreased to $1/e$ of its initial value. In other words, an electron travels a distance λ_{mfp} before it has a reasonable probability of colliding with an atom. For electrons of velocity u**,** the mean time between collisions is given by

$$\tau = \frac{\lambda_{mpf}}{u} \tag{1-9}$$

1.8: Collision Frequency

The 'collision frequency', namely the inverse of τ**,** is usually defined in terms of an average over all velocities in the Maxwellian distribution (which may have different individual collision frequencies), namely

$$\nu_c = \langle \frac{1}{\tau} \rangle \tag{1-10}$$

The velocity distribution of particles within a plasma is given, under equilibrium conditions, by a Maxwell distribution. The mean velocity $\bar{u}$ is defined by the thermodynamic temperature

$$\bar{u} = \sqrt{\frac{8kT}{\pi m}} \quad ; \quad \bar{u}^2 = \frac{3kT}{m} \tag{1-11}$$

Without applied strong magnetic fields a particle in a plasma moves between two collisions in a force-free fashion, i.e. with constant speed $\bar{u}$**.** The relaxation time τ between two collisions is:

$$\tau = \frac{\lambda_{mfp}}{\bar{u}} \sim \frac{T\sqrt{T}}{n} \tag{1-12}$$

and for the collision frequency ν_c we obtain

$$\nu_c = \tau^{-1} = \frac{\bar{u}}{\lambda_{mfp}} \tag{1-13}$$

or in terms of the collision cross-section,

$$\nu_c = n\bar{u}\sigma(v) \tag{1-14}$$

where n_a is the number density of the neutral gas, $\bar{u}$ is the thermal speed of charged particles, and σ is the collision cross-section with neutral atoms [18].

1.9: Plasma Parameter

Introducing the plasma parameter $\Lambda \approx l_L/\lambda_D$ and using the expressions for the Langmuir frequency ω_p the Debye length λ_D and $kT \approx m\bar{u}^2$ it follows [19]

$$\Lambda \approx \frac{\lambda_D}{\lambda_{mfp}} \approx \frac{\nu_c}{\omega_p} \tag{1-15}$$

1.10: Fusion Fundamentals

Fusing two atomic nuclei together can cost or release energy, depending on the mass of the resulting nucleus. For nuclei more massive than Fe-56, fusion costs energy, and therefore fission is used for mass-energy production. For nuclei lighter than ^{56}Fe, the mass of the fused

nucleus is smaller than the sum of the separate nuclei, and the excess energy is released according to Einstein's $E = \Delta mc^2$. This energy is released as heat (primarily carried by neutrons in ordinary fusion reactors) and can be used to boil water to move turbines and generate electricity.

In order to fuse two nuclei, very high energies are needed because the Coulomb barrier must be overcome. Because this barrier is directly proportional to the atomic number Z of each of the two fusing nuclei, the fuel used in fusion reactors usually consists of a combination of hydrogen isotopes (protium, deuterium and tritium) to be fused into helium isotopes.

Because of the high temperatures required for fusion, the atoms in the fuel are highly ionized and form a plasma. Plasma physics plays therefore a major role in the design of fusion reactors. In order to operate a fusion reactor continuously, the energy losses must be overcome by keeping the temperature of the fusion products sufficiently high. The Lawson criterion expresses the minimum product $n_e T \tau_E$ (called triple product) required to sustain fusion for a given reactor design, where n_e is the plasma electron density, T is the plasma temperature and τ_E is the confinement time (rate of energy loss) [20].

Instead of trying to stabilize and confine the plasma as in an ordinary fusion reactor, the Dense Plasma Focus takes advantage of the plasma natural instability to release a large amount of energy in a very short time.

Dense Plasma Focus (DPF) is a promising reactor design for achieving aneutronic fusion. A fusion reaction is called aneutronic if less than 1% of the released energy is carried by neutrons. Recent theoretical and experimental advances have raised the question of whether DPF could be the key to practical fusion power production [21]. The dense plasma focus can also be used for applications such as X-ray lithography, and in the case of higher neutron yield fuels, as a neutron source for medical applications or nuclear weapons.

1.11:Literature Survey

There exists many experimental and theoretical studies about the dense plasma focus device involving all accruing the physical phonemes. This study begins from 1960's and up to now in our work we constrict only on information for thesis studies from 1970's in order to point out as need is possible only the recently published study.

- Decker G. et al in (1980) have presented the numerical and experimental studies concerning an increase of the effective discharge current for the plasma focus from a bank of constant energy [22].

- Gerdin et al in (1981) have used the design and performance of a Faraday cup in time –of –flight technique to measure the energy spectrum of ions accelerated away from the anode of plasma focus which are described[23].

- Stygar W. et al in (1982) have used particle beam diagnostic tools involving an ion beam Faraday cup, an electron beam Faraday cup, an electron magnetic spectrometer and solid – state nuclear track detectors to measure the parameters of the particle beams generated by a Mather type dense plasma focus [24].

- Hill R.A. et al in (1983) have developed a dense plasma focus device that can be fired repetitively without purging the test gas between shots [25].

- Bilbao L. et al in (1984) have suggested a possible explanation to account for the previously observed existence of pressure dependent regimes during the implosion phase of plasma focus devices, in terms of viscous dominated Rayleigh - Taylor in stabilities [26].

- Baltog I. et al in (1985) have used A Mach –Zehnder interferometer with pulsed nitrogen laser for electronic density studies in the plasma focus device which is described [27].

- Kato Y. et al in (1986) have showed experimentally that a plasma produced from a mixture of hydrogen and a rare gas such as neon,

argon, or krypton is an effective source of a characteristic X-ray of the rare gas by plasma focus device was used [28].

- Jager U. et al in (1987) have studied the strong suprathermal fusion production of both dynamic phases of the plasma focus POSEIDON (w_0=280KJ ,U_0 = 60kV, Mather type) is considered to be due to the fast accelerated deuterons gyrating in pinch structures [29].

- Sadowski M. et al in (1988) have studied angular- and energy – distributions of ions emitted from different plasma – focus (PF) devices of energy capacity ranging from 3.6 KJ to about 200 KJ are presented [30].

- Zambreanu V. et al in (1992) have proposed a model for the trajectories of the deuteron ions in a configuration of self – consistent electromagnetic fields starting from an empirical plasma model which describes the plasma focus collapse and column phases [31].

- Kato Y. in (1994) has investigated the life time of electrodes and the insulator in a plasma focus device for application to short-wavelength radiation sources [32].

- Kelly H. et al in (1995) have analyzed the influence of multiple scattering of ions in the derivation of the ion spectrum from a Thomson ion spectrometer in a plasma focus discharge [33].

- Zakanllah M. et al in (1997) have studied the effects of the magnetic probe presence near the focus region on the current sheath dynamics [34].

- Aliaga- Rossel et al in (1998) have identified for the first time that in a medium energy plasma focus device, the neutron emission is composed of two periods, similar to that reported in high energy device [35].

- Choi et al in (1999) have investigated X-ray radiation characteristics of the plasma focus with inverse pinch switch. The plasma focus device power with capability of 20 kJ contains a 40 kV condenser power

supply and adopts a new type of switch system, the mechanism of X-ray radiation was analyzed using a pair of detectors [36].

- Vladimir A. et al in (2000) used a dense plasma focus device NX2, withinsulator, electrode, switching configuration, and with Argonfilling to concentrate the main part of its radiation near 4 A. It can be used as a source for different aims in micro – lithography [37].
- Aleksandr V. et al in (2001) presented a various designs of several medium and small size dense plasma focus (DPF) chambers intended for numerous applications, a description of technologies used in these facilities and some results reached with these devices by using a number of diagnostic techniques and had been DPF used mainly as an X-ray source [38].

- Constantin P. A in (2002) presented the result of the investigation of the electron and x – ray emission from a Mather type $3\ \mathrm{kJ}$ plasma focus device operated in Neon, carried out at $14\ \mathrm{kV}$ charging voltage, with operating pressures in the $1.5 - 5.5\ \mathrm{mbr}$range [39].
- J. Pouzo et al in (2002) were measured fast electron beams into a hollow anode of a small plasma focus machine ($2\ \mathrm{kJ}$,$4\ \mu\mathrm{F}$) [39].

- Randy H.P.Y. et al in (2003) reported the successful optimization of focus device as efficient neutron and hard X – ray source. The insulator sleeve length and deuterium filling gas pressure affect the total neutron yield from focus device [40].

P. Silva et al in (2003) presented the neutron emission from a small and fast plasma focus operating in deuterium. The system operates at low energy in the hundred of joules range ($880\ \mathrm{nF}$ capacitor bank, $38\ \mathrm{nH}$, $20–35\ \mathrm{kV}$, $176–539\ \mathrm{J}$, $\sim 300\ \mathrm{ns}$ current rise time) [41].

- H. Bhuyan et al in (2004) reported an investigation on the soft X – rays emitted in a 2.2 kJ Mather – type dense plasma focus device using a multichannel diode spectrometer and a simple pinhole camera [42].

- L. Sote et al in (2004) researched the experimental facilities in order to study fast dense transient discharges in a wide range of energy and current, energy from hundred of kilojoules to tens of joules, current from mega amperes to tens of $\mathrm{k\,amperes}$ [43].

- S. L. YAP et al in (2005) studied the Neutron emissions in a low energy $3.3\ \mathrm{kJ}$ ($15\ \mathrm{kV}$) operated in deuterium and deuterium – argon admixtures plasma focus [45].

- T. Zhang et al in (2006) conducted experiments on $2-3\ \mathrm{kJ}$ dense PF with modified anodes to show that this drive parameter remains fairly constant for the different ratios of the anode length to anode radius. It is also suggested that there may be significant differences in the values of drive parameters for Filippov – type focus devices, Mather – type focus devices, and also hybrid – type devices [46].

- V AGribkov et al in (2007): Electron and ion beam dynamics of the PF-1000 facility were investigated for the first time at its upper energy limit ($\approx 1\ \mathrm{MJ}$) in relation to neutron emission, the pinch's plasma characteristics and some other parameters with the help of a number of diagnostics with ns temporal resolution [47].

- S. Lee and S. H. Saw in (2008) used a design and simulate experiments the Lee model couples the electrical circuit with plasma focus dynamics, thermodynamics, and radiation [48].

- S. Lee et al in (2008) described how I_{pinch} may be computed from the I_{total}trace by fitting a computed current trace to the measured current trace using the Lee model [49].

- S. Lee in (2008) showed numerical experiments with no saturation; both pinch currents and neutron yield Y_n continue to rise with capacitance C_0 although at a slower rate than at lower energies. Conditions to achieve Y_n of 10^{13} in a deuterium plasma focus are

found from numerical experiments, at storage energy of $3\ \mathrm{MJ}$ with a circuit peak current of $7.6\ \mathrm{MA}$ and focus pinch current of$2.5\ \mathrm{MA}$ [50].

- S L YAP et al in (2008) presented experimental study of the dynamics of the plasma in a plasma focus device is carried out in a $3\ \mathrm{kJ}$ plasma focus. Results obtained are analyzed and fitted with the computation results obtained by using the Lee Model plasma focus modeling package [51].

- S Lee and S H Saw in (2008) presented experimental data of neutron yield Y_n against pinch currentI_{pinch}. It is assembled to produce a more global scaling law than available. From the data a mid – range point is obtained to calibrate the neutron production mechanism of the Lee Model code [52].

- S Lee et al in (2009) carried out numerical experiments, using Lee model code, incorporating a beam–target mechanism to compute the Y_n versus pressure data of plasma focus devices PF – 400 J and FN – II [53].

- R. Verma et al in (2009) reported the effect of two different cathode structures – tubular and squirrel cage, on neutron output from a miniature plasma focus device [54].

- M AMohammadi et al in (2009) studied the effect of three different anode shapes, flat, tapered and hemispherical, on the X – ray emission characteristics of a neon filled UNU–ICTP plasma focus device [55].

- S. H Saw et al in (2009) a $3.3-\mathrm{kJ}$ plasma focus, was designed for operation in deuterium with a speed factor such that the axial run – down time matches the current rise time at an end axial speed of nearly $10\ \mathrm{cm/\mu s}$ [56].

- M. Shahid Rafique et al in (2010) studied the time resolved emission of neutrons and X – rays. It was correlated with the current sheath evolution during the radial phase of a $3.2\ \mathrm{kJ}$ Mather type plasma focus device operated in deuterium at an optimized pressure of$4\ \mathrm{mbar}$ [57].

- T K Borthakur and A Shyam in (2010) observed intense burst of neutrons from a $5\ \mathrm{KJ}$ Mather type plasma focus device operated in a pressure of around $0.4\ \mathrm{torr}$ of deuterium medium in axial direction. The axial neutrons emitted from the device appear to be influenced by deuteron ion emitted in same direction [58].

- S. Zapryanov et al in (2011) measured the basic characteristics of the dense plasma focus device, namely the discharge current derivative, the soft X – ray and the hard X – ray emission from the plasma [59].

- A Tarifeño-Saldivia at el in (2011) studied the dynamics in the radial phase and plasma conditions in the pinch phase using interferometry in a plasma focus device that operates in the range of tens of joules of stored energy in the capacitor bank and tens of kilo – amperes, PF-50J [60].

- S. Lee in (2012) carried out computational and experimental studies made on the UNU/ICTP PFF in a concept of speed enhancement for neutron yield and an application of SXR for microelectronics lithography [61].

- S Lee et al in (2012) used the 6 – phases of Lee model code to fit the computed current waveform to the measured current waveform of INTI PF ($2.2\mathrm{kJ}$ at $12\ \mathrm{kV}$), a T2 plasma focus device, operated as a source of neon SXR with optimum yield around $2\ \mathrm{Torr}$ of Neon [62].
- A. Salehizadeh et al in (2013) studied the design and construction of the first Iranian $115\ \mathrm{kJ}$ Mather type plasma focus (PF) machine (IR – MPF – 100). This machine consists of a $6.25\ \mathrm{cm}$ radius and $22\ \mathrm{cm}$ height brass made anode with a $50\ \mathrm{mm}$ height insulator which

separates the anode and cathode electrodes. Twelve copper made $22\,\mathrm{cm}$ height rods play the role of cathode with $10.2\,\mathrm{cm}$ radius. Twenty four $6\,\mu\mathrm{F}$ capacitors were used with the maximum charging voltage of $40\,\mathrm{kV}$ (maximum energy of$115\,\mathrm{kJ}$) as the capacitor bank and maximum theoretical current around $1.224\,\mathrm{MA}$. The total inductance of the system is$120\,\mathrm{nH}$. By using NE – 102 plastic Scintillator, Rogowski coil, current and voltage probes, hard X – ray, current derivative, current and voltage signals of IR – MPF – 100 [63].

- M. Afsharmanesh and M. Habibi et al in (2013) studied the time – resolved of soft and hard X – ray were carried out over a wide range of argon pressures by employing an array of eight filtered photo PIN diodes and a scintillation detector, simultaneously [64].

- J. L. Ellsworth et al in (2014) used a kJ – level capacitor bank and a hollow anode, and fueled by a cylindrically symmetric gas puff have designed and built a Dense Plasma Focus (DPF) Z-pinch device. Using this device, they have measured peak deuteron beam energies of up to $400\,\mathrm{keV}$ at $0.8\,\mathrm{kJ}$ capacitor bank energy and pinch lengths of$\sim 6\,\mathrm{mm}$, indicating accelerating fields greater than$50\,\mathrm{MV/m}$ [65].

- E. Fogliatto et al in (2014) presented a planar-piston model of the hard x –ray production in Plasma Focus devices. The model applies Von Karman approximations to represent the inner structure of the pinch [66].

1.12 Aim of present work

The aim of this work is to design theoretically a dense plasma focus device and study the various parameters that affect its behavior as if it were built in the future. It is well known that the dense plasma focus is a promising reactor design for achieving aneutronic fusion. In this fusion reaction the neutrons carry a part of the released energy. Therefore the study involves the neutron yield that will produce by the system. In this wayone can decide to choose deuterium to be used as a working gas in the device. Further the study will include the effect of varying gas pressure on the entire parameters of interest. Hence one can point out to the certain pressure where the neutrons yield has the greatest value. The fact that the system will be theoretically designed using mathematical equations, thus the device will be compared with a standard system close to in the design. The behavior of the two systems would be compared graphically in terms of some important parameters.

CHAPTER

TWO

Dense Plasma Focus

2.1: Introduction

A well – known plasma device, plasma focus (PF), has been studied for a few decades. Plasma focus is amongst the few devices of thermonuclear fusion research that give high neutron and X – ray yield. Plasma focus devices take interest for their simple geometry, pulsed characters and low cost. Further, one can easily operate them as sources of neutrons, electron and ion beams as well as X – rays depending on the operating gas and reactions [67].

The dense plasma focus (DPF) or just dense plasma or also plasma gun is a plasma machine that produces, by electromagnetic acceleration and compression, a short – lived plasma that is so hot and dense that it becomes a copious multi – radiation source. It is a machine that form of electromagnetic shock tube which causes rapid compression and heating of the plasma during a fast coaxial pinch called a focus. The electromagnetic compression of the plasma is called a "pinch". The gas in a plasma focus may reach densities of 10^{19} to $10^{20}\,\mathrm{cm}^{-3}$ and temperatures of a few keV during the several hundred ns long pinch [68]. The device characteristics produce short – lived plasma that hot and dense enough to cause nuclear fusion and the emission of X – rays.

2.2: Mather vs. Filippov type device

Historically, the dense plasma focus was discovered independently by Fillipov et al. in 1954 (in the former Soviet Union)[69] and shortly by Mather in the early $1960\mathrm{s}$ (in the USA) [70], who used a coaxial gun geometry. Although the devices investigated by these two pioneers had significantly different geometries. Many plasma focus devices have since been built by other investigators, but all broadly conform to one of the two original geometries, and can be classified as being either of the Mather or Filippov type.

The operating principle of both the devices is the same expect for some differences: basically they differ in the geometric design, where the former Mather type is adjusted vertically while Filippov type is adjusted horizontal. Also they are different in the dimension of the

inner and the outer electrodes plasma and the aspect ratio (diameter/length) of inner electrode. The aspect ratio of Mather type is smaller than one and of the Filippov type is greater than one [71] which affect the macroscopic direction of motion of the accelerated plasma (axial and radial, respectively).

The most striking difference from the Mather design is the absence of a coaxial length to accelerate the plasma. The plasma is generated in the same way as the Mather device, and the pinch phase is similar, but the Filipov-type device lacks an acceleration phase. Immediately after breakdown, the plasma sheath sweeps along the outer electrode towards the axis and pinch begins almost immediately. The two devices produce similar results. However, the Filipov device is of considerably larger radial dimensions, being 48 cm for the inner electrode and 70 cm for the outer electrode. Geometries for both type of dense plasma focus device are illustrated in Figure 2.1 .

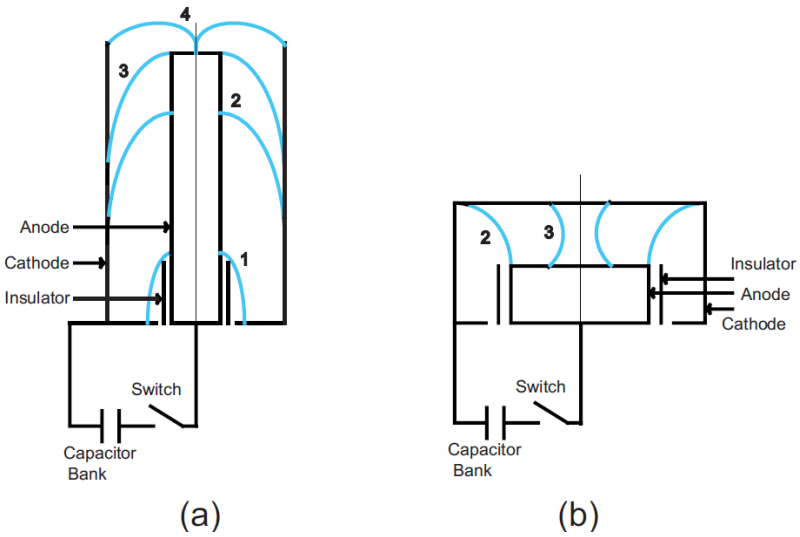

Figure 2.1: Schematic of a) Mather – type and b) Filippov – type dense plasma focus device [72].

For reference, the axial direction refers to the z-axis. The two configuration show the formation of the plasma from flashover of the insulator1, followed by the sheet propagation 2,3 through collapse of the current sheets to form the pinch 4 [73].

However, these devices have been built with stored bank energy ranging from 1 kJ to 1 MJ with consequent variation in the physical sizes of the device [74]. Both of them include mainly three individual phases when they operate. First phase is the initial gas breakdown which constructs a current sheath. Second one, namely acceleration phase forms the plasma and pushes it by the Lorentz force toward the open end of the electrode. The last phase of the discharge is the collapse of the current sheaths as a pinch form.

The coaxial discharge arrangement in a plasma focus devices uses a fast rising current pulse with the inner electrode as anode and the outer electrode as cathode. The plasma discharge is initiated along a dielectric insulator at the closed, upstream end of the electrode assembly and generates a $\mathbf{J} \times \mathbf{B}$ Lorentz force that drives the plasma sheath toward the open end of the coaxial electrode assembly. Once the plasma sheath has traversed the length of the anode, magnetic forces rapidly further accelerate the plasma radially inward across the face of the anode, resulting in the formation of a pinched plasma column with very high temperature and density [75].

The "pinch" compression should coincide with the peak current for the best efficiencies. This pinch produces beams of ions, electrons, neutrons and short X-rays pulses. The radiation and particle beams produced by the device can be varied by changing the operating gas, e.g. using deuterium as the gas, fast neutrons and proton beams are produced.

2.3: Division of Dense plasma focus

Dense plasma focus (DPF) devices can be divided according to operation and energy as follows [76]:

1- Conventional devices: The energy ranges from a few kilojoules to mega – joules, producing neutron pulses from 10^7 to 10^{12} neutrons per shot. Currently more laboratories are equipped with Mather type DPF devices. A few laboratories are still working with Filippov type DPF devices.

2- Repetitive devices: These plasma focus (PF) devices are used for X – ray production with $2-5\,\mathrm{kJ}$ electrical energy stored in the capacitor bank and a repetition rate on the order of $2-16\,\mathrm{Hz}$.
3- SPEED devices: SPEED devices are generators based on Marx technology. They were designed at the University of Düsseldorf. Those devices drive a fast plasma focus where the maximum current is achieved in $400\,\mathrm{ns}$ or less. The special design produces a device with an impedance on the order of the pinch impedance ($\sim 100\,\mathrm{m\Omega}$), making it more efficient in the transference of the energy to the plasma.
4- Compact devices with energy lower than $1\,\mathrm{kJ}$. Lower energy range constitutes an area of research that is not well explored for plasma focus devices. Some DPF devices were constructed with tens to a few hundred joules of stored energies. These very small devices produce pulses of pinch plasmas, neutrons and X – rays.

2.4: The main features of the plasma focus devices

In general, the main features of the plasma focus devices are [77]:

1- The capability of producing a combination of intense pulses of hot plasma, neutrons, fast electrons and ions, and soft and hard X-rays.
2- Relatively simple operating principle and construction, cost effectiveness, and easy maintenance.
3- Ecologically clean compared to other types of sources.
4- Short emission time on the order of tens of ns.
5- Small source size in the order of mm^3.

2.5: Plasma Focus Dynamics

As mentioned above the plasma focus dynamics is divided into three main phases, the breakdown phase, the axial acceleration phase, and the radial collapse phase. In next sections we review the dynamic of plasma focus.

2.5.1: Breakdown Phase

When high voltage is applied between the coaxial electrodes which cause the filling gas to breakdown a discharge is initiated and forms a plasma sheath in which the discharge current circulates [78]. The initial breakdown starts from the center electrode along the insulator to the end – plate portion of the outer electrode. The breakdown striated light pattern which forms a few tenths of a microsecond after application of the breakdown voltage [79]. As the current to the electrodes increases at a rate determined by the ringing frequency of the system, the filamentary pattern at the breech begins to move radially outward from the insulator until it reaches the cylinder part of the outer electrode. This effect has been called the inverse pinch effect because magnetic forces cause the plasma sheath to expand instead of pinch.

Upon formation of the current sheath, it will be lifted off from the insulator surface. The initial current sheath near the insulator surface is thick and it propels radially outwards in an inverse pinch manner by the $(\boldsymbol{J} \times \boldsymbol{B})_r$ force until it reaches the outer electrode. When a uniform current sheath in cylindrical shape is formed, this marks the end of the breakdown phase. The breakdown and formation of current sheath also depends on the operating pressure [80]. At very low pressures, the discharge can develop within the whole inter electrode volume. On the other hand, at very high pressures, a radial filamentary discharge occurs between the coaxial electrodes [81]

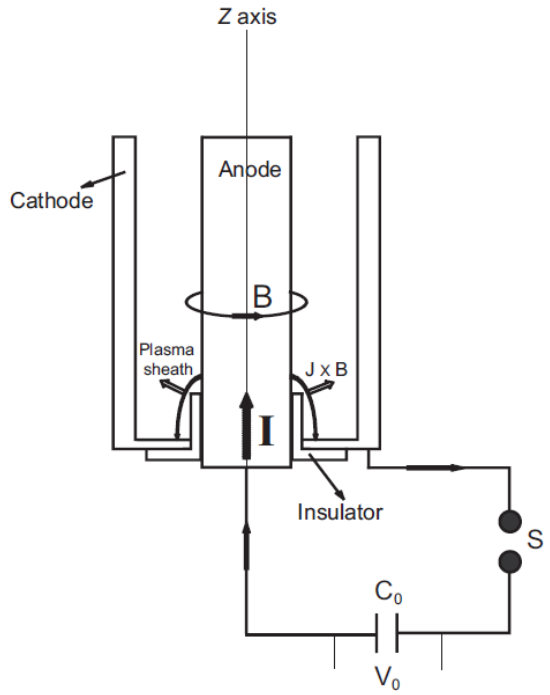

Figure 2.2: break down phase [82,83].

It should be remarked here, that the optimization of the anode and cathode separation and also length of the insulator and initial gas conditions have a great influence on uniformity of breakdown discharges [83].

It has been experimentally shown [84] that if the current sheath does not become azimuthly symmetric but instead develops a preferred radial filament, the neutron yield from a deuterium gas filled plasma gun is very poor or still missing [85].

2.5.2: The Acceleration Phase

The next phase of the evolution of plasma focus discharge is known as the axial run-down phase or simply, run-down phase. The current sheath formed at the end of the breakdown phase is accelerated by its own $(\boldsymbol{J} \times \boldsymbol{B})$ force towards the open end of the inner electrode along the insulator [86]. This phase does not exist in the Filippov type plasma focus devices due to a short anode length.

The total acceleration force $\boldsymbol{J} \times \boldsymbol{B}$ acting perpendicular to the current boundary leads to radial and axial motion. The $(\boldsymbol{J} \times \boldsymbol{B})_r$ radial

component is outward and forces the current sheath to be annular at the outer electrode. The axial force$(\boldsymbol{J} \times \boldsymbol{B})_r$ varies $1/r^2$ across the annulus and leads to higher sheath velocities near the surface of the center electrode. This is proved by measurements by using magnetic probes [87].

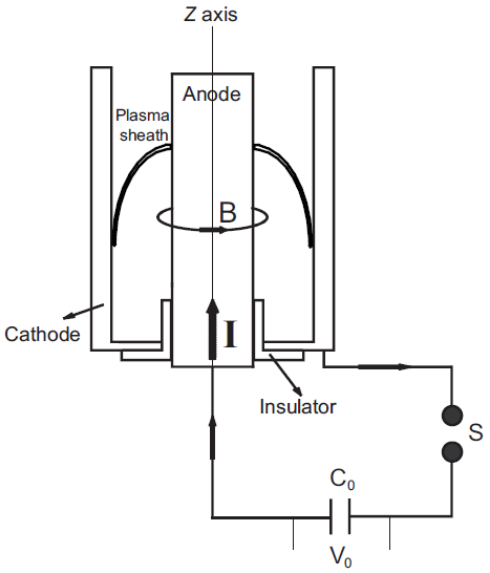

Figure 2.3: acceleration phase[83].

At the end of this phase, one end of the current sheath sweeps around the end of the anode. The outer end of the current sheath continues along the tube sweeping along with it the greater portion of the accumulated plasma in the axial direction. Only a fraction of plasma at the end of axial acceleration phase contributes to the final focus [88].

The following are the two conditions that make the axial phase important for the subsequent formation of the hot and dense plasma.

1. The first condition is that the current sheath should arrive at the axis in coincidence with the first maximum of the discharge current. This condition is a common requirement to all the pinch devices. It represents the optimization of the energy transfer from the capacitor bank to the pinch plasma.
2. The second condition is that the structure and the (r, z) profile of the plasma sheath should have certain characteristics for a good

focusing effect. This condition requires an axial symmetry, smooth (r, z) profiles and a thin uniform current sheath structure [89].

Predicting the time of arrival of the current sheath allows tailoring of the dense plasma focus system parameters such as gas – filling pressure, applied voltage, and center electrode length to produce a plasma focus coincident with the maximum bank current. By synchronizing the focus with the maximum sheath current, the energy stored in the magnetic field, which drives the pinch phase, can be maximized, thereby increasing x-ray and neutron production.

Two important phenomena take place in axial acceleration phase, namely the current shedding and mass loss. Current shedding is the loss of discharge current during the current sheet movement. On the other hand, mass loss is the escape of mass, carried by current sheet, through the transparent outer electrode. The current shedding occurs due to the slow moving diffused current layer behind the main current sheet and the current retained by insulator surface whereas mass loss results from the pressure gradient in the canted current sheet. The mass loss can be realized from the decrease in current sheet thickness as it moves towards the open end of the electrode [90].

2.5.3: Collapse Phase

The third phase encompasses the rapid convergence of the plasma sheath to the axis and the conversion of stored magnetic energy to plasma energy in the focus. The (r, z) convergence is due to the $\boldsymbol{J} \times \boldsymbol{B}$ pinch phase. With this configuration, there is no equilibrium along the axis, hence, the plasma may readily escape axially in either direction. By the very nature of the convergence, much of the gas that the plasma sheath encounters during collapse is ejected downstream and lost. The gas trapped in the focus is estimated as $\sim 10\%$ of that originally percent.

The pinch effect is perhaps the most efficient way of heating and compressing a plasma. As the pinch induced implosion velocity of the current boundary imparts the same velocity to both ions and electrons, and because of the ion-electron mass difference, most of the energy

appears as kinetic energy of the ions. In pinch devices, the ions are preferentially heated.

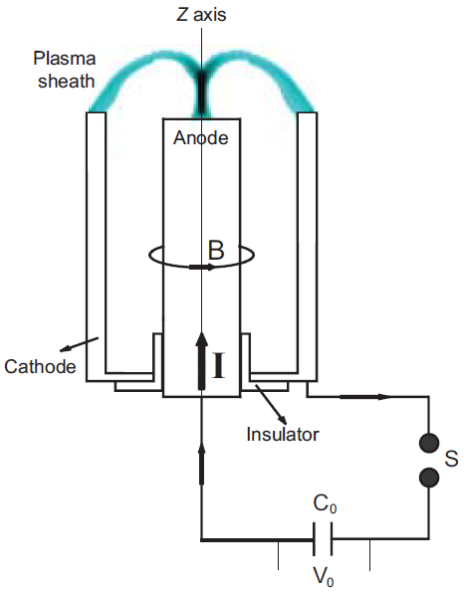

Figure 2.4: collapse phase [83]

The radial phase could be divided into four sub-phases: (a) compression phase (b) quiescent phase, (c) unstable phase and (d) decay phase.

2.5.3.1: Compression phase

This phase begins just after the arrival of the current sheath to the end of the inner electrode as it starts to sweep around the end of the electrode. The phase evolves as the sheath collapses radially inward forming an azimuthally symmetric, non-cylindrical, funnel-shaped towards the axis under the influence of the inward $\boldsymbol{J} \times \boldsymbol{B}$ force [91].

At the beginning of this phase, the length of the plasma column is considered zero while its radius is considered same as the anode radius. As it pinches inwards, the length of the plasma column elongates while the radius becomes smaller. In this phase, the plasma is compressed adiabatically thus forming a very high temperature and high density plasma column. Heating and compression of plasma can be achieved due to the pinch effect. However, this will lead to rapid growth of hydro-

magnetic instabilities radially inward propagating precursor shock wave is formed in this phase.

The compression phase ends when the plasma column reaches a minimum radius (maximum compression) and the plasma density is maximum ($\sim 10^{19}\mathrm{cm}^{-3}$). It is difficult to obtain a uniform plasma column because of this instability. At the end of this phase, the inductance of the system becomes maximum because the plasma column radius reaches its minimum [92].

2.5.3.2: Quiescent phase

This phase starts when the compressed plasma focus column begins to expand. The expansion takes place in both axial and radial directions. The rate of expansion in the radial direction is hindered by the confining magnetic pressure. But the plasma can expand unhindered in the axial direction due to the fountain-like geometry of the current sheath. Thus, an axial shock front is form.

In this phase, an energy exchange occurs between ions and electrons owing to the temperature difference among them where electrons were colder than the ions. Due to this collisions process in the plasma column, the dimension of plasma column starts to expand rapidly. Because the total number of ions and electrons remained constant in this phase, the particle density drops as the plasma expands. The phase usually last for about 30 ns. The sudden change of inductance induces a high electric field that will accelerate the ions and electrons. Thus, electrons and ions are emitted in opposite direction. The induced electric fields are to maintain the current flow in the plasma column towards the end of this phase; $m = 0$ instabilities start to grow [93].

At the end of the quiescent phase, the $m = 0$ instability develops rapidly due to the increase of electron temperature. The plasma column is locally compressed again due to the $m = 0$ instability. The pinch lifetime which is defined as the time between the first compression and the instant when the *m*=0 instability occurs, affects the emission characteristics of DPF device: the shorter the pinch life time, the higher the neutron yield for fixed DPF discharge parameters.

2.5.3.3: Unstable phase

The unstable phase is the richest stage of the plasma focus evolution in associated phenomena like soft and hard x-ray emission, fast deuterons and electrons and $D-D$ reaction products (neutrons, protons) if operated in deuterium. Figure 2.5 shows a schematic of the emission of the radiation from the plasma focus after the focusing event. Due to the growth of the $m=0$ instability, the induced electric field is enhanced. This accelerates the electrons towards the inner electrode (anode) and the ions in the opposite direction.

A fairly large amount of impurities is injected into the plasma column due to the bombardment of accelerated runaway electrons on the anode. The explosion proceeds sequentially along the plasma column [64]. The disruption of the plasma column continues until the whole plasma column is broken completely broken up, and the plasma density decreases.

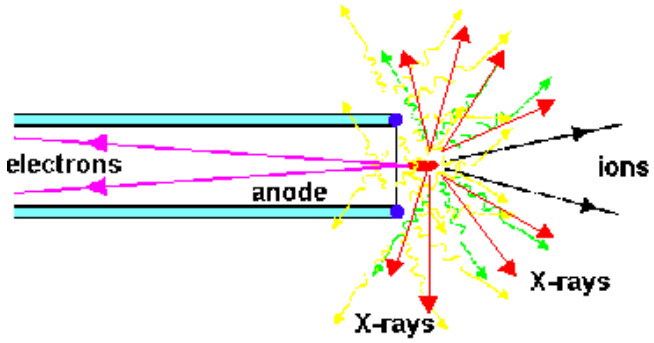

Figure 2.5: Emission of radiation from the focus [95].

2.5.3.4: Decay phase

The last phase of the radial collapse and also the last stage of the plasma focus dynamics is the decay phase. During the decay phase a large, hot and thin plasma cloud is formed due to the complete breaking up of the plasma column. This plasma cloud emits a large amount of Bremsstrahlung radiation. The soft X-ray emission rises abruptly during the decay. At this stage, the neutron pulse that starts from the beginning of the unstable phase reaches its peak value.

The whole process usually lasts tens of nanoseconds for a small focus (several kJ) to a fraction of microsecond for a large focus device (Mega Joule).

2.6: Applications of plasma focus devices

There are a large number of possible technological applications for the plasma focus at different stages of development. A dense plasma focus installation, explored mostly within the fusion program, is known as a powerful neutron, very broad X-ray spectrum generator and ion or electron source. At the same time the DPF is able to operate with some types of gas or gas mixtures, becoming a generator of a pure X-ray radiation, not accompanied by the neutrons. As an X-ray radiation generator the DPF has two principal distinctive features.

The first one is the X-ray pulse shortness, and the second one is an extremely great power of the x-ray pulse. These features accompanied by DPF x-ray spectrum peculiarity give an opportunity to apply a DPF installation (even of a small dimension class) into a number of branches of science and technology, where other X-ray sources cannot be used.

On the other hand, when PDF devices work with deuterium gas, it can be used as a high power neutron source. The particular characteristics of this neutron source are:

1) High neutron emission rates up to 10^{18} -10^{19} neutrons/s.

2) Neutron emission duration of about 10^{-7} s, with large variations on a time scale of about 10^{-9}s.

3) Average neutron energy around $2.45\ \mathrm{MeV}$, the neutron energy spectrum having a full width at half maximum (FWHM) of a few 100 keV.

4) The neutron energy spectrum is expected to have both time and space dependence.

These abilities make plasma focus devices as a suite device for basic investigations, industrial and bio-medical applications, new technology development, etc. Among the most interesting plasma focus applications we could mention as following: [96, 97]

a) Controlled thermonuclear fusion
b) Short and intense Neutron sources for inspection of nuclear materials (uranium, plutonium).

c) Pulsed X-rays sources.
d) Application of a high repetition rate and high efficiency plasma focus for nanotechnologies, including X-ray nano – lithography for microelectronics and micromachinery.
e) X-ray microscopy.
f) Production of short life radioisotopes.
g) Radiography with neutrons.
h) Ions implantation.
i) Spectroscopy of highly charged ions.

2.7: Radiation Emission From Dense Plasma Focus Device

Different types of radiations are emitted from hot plasmas. These radiations include electromagnetic radiations, neutrons, electrons and ion beams as well as high energy neutral particles, which are atoms and molecules. Considerable efforts have been concentrated from the discovery of the plasma focus on the study of the emission of radiation like neutrons, X-rays (hard and soft) and charged particles. Also, special attention has been paid to study the current sheath structure, its dynamics, pinch formation and role of MHD instabilities in the emission of radiation. The general properties of DPF discharge such as, neutron emission times, energy spectra, and X-ray emission were first studied by Mather and Bernstein [98].

CHAPTER

THREE

Lee Code

3.1: Introduction

The Lee Model simulates a conventional Mather-type plasma focus by inputting machine parameters; inductance, capacitance, electrode radii and length and operating parameters; charging voltage, gas type and fill gas pressure. The thermodynamics (specific heat ratio and charge number as functions of temperature) for 6 gases namely hydrogen, deuterium, neon, argon and helium and xenon are included. The gases may be selected by simply inputting atomic number, molecular weight and dissociation number (2 for deuterium, 1 for the others) [98].

The Lee model code couples the electrical circuit with plasma focus dynamics, thermodynamics, and radiation, enabling a realistic simulation of all gross focus properties [99]. The basic model, described in 1984 [100]. The model also contends that most important properties of the plasma focus may be deduced from the discharge or pinch current flowing in the device.

The description, theory, code, and a broad range of results of this model are available for download from the "Universal Plasma Focus Laboratory Facility" [101] In addition; the mechanics of fitting the model to a measured current trace which is described in the Internet Course notes is also available.

A recent additions is the inclusion of the neutron yield, Y_n, using a beam-target mechanism [102,103], incorporated in recent versions of the code (versions later than RADPFV5.15) [104], A beam of fast deuteron ions is produced by diode action in a thin layer close to the anode, with plasma disruptions generating the necessary high voltages. The beam interacts with the hot dense plasma of the focus pinch column to produce the fusion neutrons [105], and plasma self-absorption of X-rays.

Information obtained from the model includes axial and radial velocities and dynamics, dimensions and duration of the focus pinch, gross information of temperatures and densities within the pinch, soft X-ray emission characteristics and yield [106], design and optimization of machines [107,108].

The demonstrated is versatility and utility of the model in its clear distinction of I_{pinch} from I_{peak} [109] and the recent uncovering of a plasma focus pinch current limitation effect.

3.2: Brief description of Lee Model

The present 5-phase package (axial, radial inward shock, radial reflected shock, slow compression radiative and expanded large column phase) is re-written in Microsoft EXCEL VISUAL BASIC in order to make it available for wider usage.

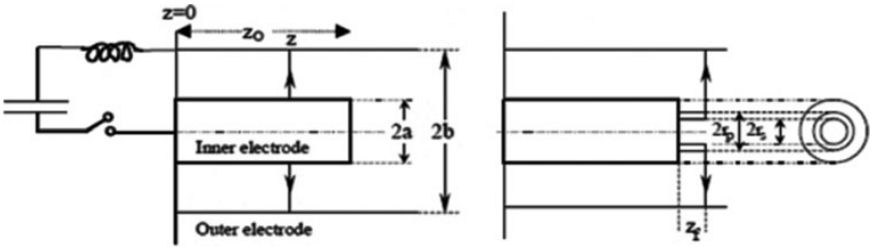

a. Axial phase b. Radial phase

Figure 3.1: Schematic of the axial phase and radial phase of the Mather plasma focus [110].

The five phases of the plasma focus that are simulated in the Lee Model code are:

3.2.1. Axial Phase:

This phase described by a snowplow model with an equation of motion coupled to a circuit equation. The equation of motion incorporates empirically the axial phase model parameters: mass and current factors f_m and f_c, respectively. The mass swept-up factor f_m accounts for not only the porosity of the current sheet but also for the inclination of the moving current sheet-shock front structure and all other unspecified effects which have effects equivalent to increasing or reducing the amount of mass in the moving structure, during the axial phase. The current factor, f_c, accounts for the fraction of current effectively flowing in the moving structure (due to all effects such as current shedding at or near the back-wall and current sheet inclination). This defines the fraction of current effectively driving the structure, during the axial phase [111]

The mass of the plasma sheath is the mass of the shocked gas in the annular channel up to position z is [112]

$$m = \{\rho_0 \pi (b^2 - a^2) f_m z\} \qquad (1-3)$$

where ρ_0 is the gas density and is assumed to be constant , a is anode radius and b is cathode radius, z is the axial position of the current sheath, f_m is fraction of mass swept down the axial direction.

The induced magnetic field between a and b

$$\left(B_\vartheta = \mu I_p / 2\pi r\right) \qquad (2-3)$$

where $I_p = f_c I$ is the current flown through the plasma, $\mu = 4\pi \times 10^{-7}\,\mathrm{H/m}$ is the permeability of space and r is the radius of the magnetic field lines

Magnetic force F on current sheath is

$$F = \int_a^b \left[\frac{\left(\frac{\mu I f_c}{2\pi r}\right)^2}{2\mu}\right] 2\pi r dr \; = \frac{\mu f_c^2}{4\pi} \ln(c) I^2 \qquad (3-3)$$

where $c = b/a$ and f_c is fraction of current flowing in the piston, I is the discharge current.

Equating the rate of change of momentum at the current sheet [113],

$$\frac{d}{dt}\left[m \frac{dz}{dt}\right] = F \qquad (3-4)$$

substituting eq. $(1-3)$ and $(3-3)$ in $(3-4)$

$$\frac{d(mv)}{dt} = \frac{d}{dt}\left(\left[\rho_0 \pi (b^2 - a^2) z\right] f_m \frac{dz}{dt}\right) = \rho_0 \pi (c^2 - 1) a^2 f_m \frac{d}{dt}\left(z \frac{dz}{dt}\right)$$

$$\rho_0 \pi (c^2 - 1) a^2 f_m \frac{d}{dt}\left(z \frac{dz}{dt}\right) = \frac{\mu f_c^2}{4\pi} \ln(c) I^2 \qquad (3-5)$$

then we have [114]

$$\frac{d^2 z}{dt^2} = \left[\frac{f_c^2}{f_m} \frac{\mu_0 (\ln c)}{4\pi^2 \rho_0 (c^2 - 1)} \left(\frac{I}{a}\right)^2 - \left(\frac{dz}{dt}\right)^2\right] / z \qquad (3-5)$$

The equation represents the equation of motion.

It incorporates axial phase model parameters: mass and current factors f_m and f_c, and is coupled to a circuit equation

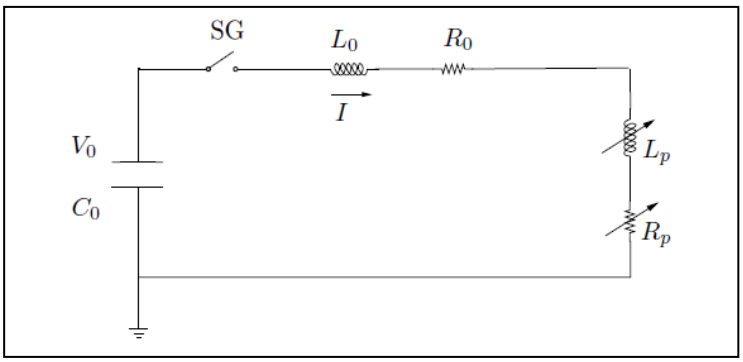

Figure 3.2: Equivalent electrical circuit for plasma focus[115].

According to Kirchhoff's second law, the equation of this circuit can be written as,

$$\frac{1}{c_0}\int_0^1 Idt - V_0 + R_0 I + \frac{d}{dt}(L_0 I) + R_p I_p + \frac{d}{dt}(L_p I_p) = 0 \qquad (3-6)$$

and the tube voltage

$$V = V_0 - \frac{1}{C_0}\int Idt - RI - L_0\frac{dI}{dt} = R_p I_p + \frac{d}{dt}(L_p I_p) \qquad (3-7)$$

Where $L_p = \frac{\mu}{2\pi} z \ln\frac{b}{a}$ is the inductance of the plasma focus tube ,V_0 is initial charge applied to the capacitor, L_0 is circuit stray inductance (H), C_0 is energy storage capacitance (F), and R_0 is stray circuit resistance (ohm) , R_p is the resistance of the plasma focus tube.

Substitute this expression into the general circuit equation Eq. $(3-6)$, we can get the circuit equations for the axial phase,

$$\frac{dI}{dt} = \frac{V_0 - \frac{1}{C_0}\int Idt - \left(R_0 + f_c R_p\right) - I f_c \frac{\mu}{2\pi}\ln\frac{bdz}{adt}}{L_0 + \frac{f_c \mu}{2\pi}\ln\frac{b}{a}z} \qquad (3-8)$$

In addition, the electrical characteristics of the circuit have the following parameters:

We also define:

$Z_0 = L_0/C_0$ (Surge impedance, ohm)

$t_0 = (L_0C_0)^{1/2}$ (Note: $2\pi(L_0C_0)^{1/2}$ is the L – C circuit cycle time)

$I_0 = V_0/Z_0$ the peak current of the L – C circuit.

This is normalized with $\tau = t/t_0$, $\xi = \frac{z}{z_0}$ and $i = I/I_0$ i.e., we replace variables t_0, Z_0, I_0 by non-dimensionalised quantities

From equation $(3-5)$ which we write as

$$\frac{z_0}{t_0^2}\frac{d^2\xi}{d\tau^2} = \left[\frac{f_c^2}{f_m}\frac{\mu \ln c}{4\pi^2 \ \rho_0(c^2-1)}\left(\frac{I_0}{a}\right)^2 \iota^2 - \frac{z_0^2}{t_0^2}\left(\frac{d\xi}{d\tau}\right)^2\right] \Big/ \xi z_0$$

$$\frac{d^2\xi}{d\tau^2} = \left[\frac{f_c^2}{f_m}\frac{\mu \ln c}{4\pi^2 \ \rho_0(c^2-1)}\left(\frac{I_0}{a}\right)^2 \frac{t_0^2}{z_0^2}\iota^2 - \left(\frac{d\xi}{d\tau}\right)^2\right] \Big/ \xi$$

$$\frac{d^2\xi}{dt^2} = \left[\frac{\alpha^2\iota^2 - \left(\frac{d\xi}{d\tau}\right)^2}{\xi}\right] \qquad (3-9)$$

where $\alpha = (t_0/t_a)$ with t_a identified as the characteristic axial transit time:

where $t_0 = \left[\frac{4\pi^2(c^2-1)}{\mu \ln c}\right]^{1/2} \frac{\sqrt{f_m}}{f_c}\frac{z_0}{I_0/a/\sqrt{\rho}}$

$$\alpha^2 = \frac{t_0^2}{\left[\frac{z^2}{(1/a)^2}\frac{f_m}{f_c^2}\frac{4\pi(c^2-1)}{\mu(\ln c)}\right]}$$

Normalizing the circuit equation$(3-8)$, we have

$$\frac{d\iota}{d\tau} = \left(1 - \int \iota d\tau - \beta\iota\frac{d\xi}{d\tau} - \delta\iota\right)/(1+\beta\xi) \qquad (3-10)$$

where $\beta = \frac{L_0}{L_a}$ is the ratio of load to source inductance and since the device is electromagnetic and $I_0/a/\sqrt{\rho}$ is the drive parameter.

where $\delta = R_0/Z_0$ is the ratio of circuit stray resistance to surge impedance. This acts as a damping effect on the current.

The axial phase is relatively unimportant for the model; its main purpose is to delay the pinch formation until the current reaches a high enough value.

3.2.2. Radial Inward Shock Phase*:*

Described by four coupled equations using an elongating slug model: The first equation computes the radial inward shock speed from the driving magnetic pressure [116].

The mass of the shocked gas at position r_s is $\pi\rho_0(a^2 - r_s^2)z_f$, where r_s is the radial shock front position, z_f Plasma slug (column) height on the anode top in radial phase.

The shock front speed can be related to the pressure according to the shock wave theory [117]

$$P_s = \frac{2}{\gamma+1}\rho_0 v_s^2 \qquad (3-11)$$

where γ is specific heat ratio of the operating gas.
The force that drives the compression is the magnetic piston, whose pressure is,

$$p_m = \frac{B^2}{2\mu_0} = \frac{(\mu I f_c/2\pi r_p)}{2\mu} \qquad (3-12)$$

Further, at the magnetic piston we may equate the pressure $\mathrm{P_s}$ to the magnetic pressure $\mathrm{P_m}$ so that [118]:

$$P_s = P_m = \frac{2}{\gamma+1}\rho_0 v_s^2 \qquad (3-13)$$

From equation $(3-11)$

$$v_s^2 = \frac{\mu(If_c)^2}{8\pi^2 r_p} \times \frac{\gamma+1}{2\rho_0 f_{mr}}$$

Thus: Radial shock speed

$$v_s = \frac{dr_s}{dt} = -\left[\frac{\mu(\gamma+1)}{\rho_0}\right]^{1/2} \frac{f_c}{\sqrt{f_{mr}}} \frac{I}{4\pi r_p} \qquad (3-14)$$

Where r_p is radial piston position, f_{mr} is modified f_m value in the radial phase.

This may be normalized with $\kappa_s = r_s/a$, $\kappa_p = r_p/a$, and $\xi_f = z_f/a$ giving:

$$\frac{d\kappa_s}{d\tau} = -\alpha\alpha_1 \iota/\kappa_p \qquad (3-15)$$

where $\alpha_1 = \frac{t_a}{t_p} = \sqrt{\frac{(\gamma+1)(c^2-1)}{4(\ln c)}}\ F\left[\left(\frac{f_m}{f_{mr}}\right)^{1/2}\right]$, $t_p = \frac{4\pi}{[\mu(\gamma+1)]^{1/2}} \frac{\sqrt{f_{mr}}}{f_c} \frac{\sqrt{\rho}}{I_0/a} a$ and $F = \frac{z_0}{a}$.

The second equation computes the axial elongation speed of the column.

$$\frac{dz_f}{dt} = -\left(\frac{2}{\gamma+1}\right)\frac{dr_s}{dt} \qquad (3-16)$$

Similarly, this can be normalized to:

$$\frac{d\xi_f}{dt} = -\left(\frac{2}{\gamma+1}\right)\frac{d\kappa_s}{d\tau} \qquad (3-17)$$

The third equation computes the speed of the current sheath, also called the magnetic piston, allowing the current sheath to separate from the shock front by applying an adiabatic approximation [119]

$$\frac{dr_p}{dt} = \frac{\frac{2}{\gamma+1}\frac{r_S dr_S}{r_p\, dt} - \frac{r_p}{\gamma I}\left(1-\frac{r_S^2}{r_p^2}\right)\frac{dI}{dt} - \frac{r_p}{z_f}\left(1-\frac{r_S^2}{r_p^2}\right)\frac{dz_f}{dt}}{\frac{\gamma-1}{\gamma}+\frac{1}{\gamma}\frac{r_S^2}{r_p^2}} \qquad (3-18)$$

It also can be applied to describe the dense plasma column in the reflected and slow compression phase.
After normalization, this becomes:

$$\frac{d\kappa_p}{dt} = \frac{\frac{2}{\gamma+1}\frac{\kappa_S d\kappa_S}{\kappa_p\, dt} - \frac{\kappa_p}{\gamma\iota}\left(1-\frac{\kappa_S^2}{\kappa_p^2}\right)\frac{d\iota}{dt} - \frac{1}{\gamma+1}\frac{\kappa_p}{\xi_f}\left(1-\frac{\kappa_S^2}{\kappa_p^2}\right)\frac{d\xi_f}{dt}}{\frac{\gamma-1}{\gamma}+\frac{1}{\gamma}\frac{\kappa_S^2}{\kappa_p^2}} \qquad (3-19)$$

The fourth is the circuit equation.

$$\frac{d}{dt}\left[\left(L_0 + L_{z_0} + L_f\right)I\right] + I\left(R_0 + R_f\right) = V_0 - \int_0^t \frac{Idt}{c_0} \qquad (3-20)$$

where $L_{z_0} = (\mu/2\pi)(\ln c)z_0$ is the inductance of the focus tube, $L_f = (\mu/2\pi)(\ln b/r_b)z_f$ is the inductance of the radially imploding & elongating plasma pinch.

Substitute these expression into the general circuit equation Eq. $(3-20)$

Thus $L = (\mu/2\pi)(\ln c)z_0 + (\mu/2\pi)(\ln b/r_b)z_f$ where both z_f and r_p vary with time.

$$\left\{L_0 + f_c\frac{\mu}{2\pi}(\ln c)z_0 + f_c\frac{\mu}{2\pi}\left(\ln\frac{b}{r_p}\right)z_f\right\}\frac{dI}{dt} + f_c I\frac{\mu}{2\pi}\left(\ln\frac{b}{r_p}\right)\frac{dz_f}{dt} - f_c I\frac{\mu}{2\pi}\frac{z_f}{r_p}\frac{dr_p}{dt} + r_0 I = V_0 - \frac{\int Idt}{C_0} \qquad (3-21)$$

and therefore that fourth of the circuit equation is :

$$\frac{dI}{dt} = \frac{V_0 - \frac{\int Idt}{C_0} - R_0 I - f_c\frac{\mu}{2\pi}\left(ln\frac{b}{r_p}\right)I\frac{dz_f}{dt} + f_c\frac{\mu}{2\pi}\left(\frac{z_f}{r_p}\right)I\frac{dr_p}{dt}}{L_0 + f_c\frac{\mu}{2\pi}(ln\, c)z_0 + f_c\frac{\mu}{2\pi}\left(ln\frac{b}{r_p}\right)z_f} \qquad (3-22)$$

The normalized form is:

$$\frac{d\iota}{dt} = \frac{1-\int \iota dt+\beta\left(\ln\frac{\kappa_p}{c}\right)\iota\frac{d\xi_f}{d\tau}+\beta\xi_f\iota\frac{d\kappa_p}{d\tau}-\delta\iota}{\left\{1+\beta-\beta_1\left(\ln\frac{\kappa_p}{c}\right)\xi_f\right\}} \qquad (3-23)$$

where $\beta_1 = \frac{\beta}{F\ln c}$

The model parameters, radial phase mass and current factors, f_{mr} and f_{cr}, are incorporated in the radial phases. Thermodynamic effects due to ionization and excitation are incorporated into these equations, these effects being important for gases other than hydrogen and deuterium. The average temperature and number densities are computed during this phase.

The four equations can then be integrated by applying a time difference, D, as follows :

$\kappa_s = \kappa_s + \frac{d\kappa_s}{d\tau}D$, $\xi_s = \xi_s + \frac{d\xi_f}{d\tau}D$, $\kappa_p = \kappa_p + \frac{d\kappa_p}{d\tau}D$, $\iota = \iota + \frac{d\iota}{d\tau}D$, and $\int \iota d\tau = \int \iota d\tau + \iota D$

The normalized voltage, $\upsilon(= V/V_0)$ can be calculated from considering only the inductive component $= d(LI)/dt$, [120]

$$V = \frac{\mu}{2\pi}\left[(\ln c)_{z_0} + \left(\ln\frac{b}{r_p}\right) z_f\right] f_c\frac{dI}{dt} + \frac{\mu}{2\pi}\left[\left(\ln\frac{b}{r_p}\right)\frac{dz_f}{dt} - \frac{z_f}{r_p}\frac{dr_p}{dt}\right] f_c I \text{ (3-24)}$$

The normalized voltage is then:

$$\upsilon = \left[\beta - \beta_1\left(\ln\frac{\kappa_p}{c}\right)\xi_f\right]\frac{d\iota}{d\tau} - \beta_1\iota\left[\frac{\xi_f}{\kappa_p}\frac{d\kappa_p}{d\tau} + \left(\ln\frac{d\kappa_p}{c}\right)\frac{d\xi_f}{d\tau}\right] \quad (3-25)$$

In addition, a communication delay between shock front and current sheath due to the finite small disturbance speed is incorporated by calculating an appropriate delay when integrating the shock speed [121].

3.2.3. Radial Reflected Shock (RS) phase:

When the shock front hits the axis, because the focus plasma is collisional, a reflected shock develops which moves radially outwards, whilst the radial current sheath piston continues to move inwards.

Four coupled equations (a, b, c, d) are also used to describe this phase, these being for the reflected shock moving radially outwards, the piston moving radially inwards, the elongation of the annular column and the circuit equation. The same model parameters f_{mr} and f_{cr} are used as in the previous radial phase. The reflected shock is estimated to be $1/3$ of the inward radial shock speed [123].

$$\frac{dr_r}{dt} = -0.33\left(\frac{dr_s}{dt}\right)_{\text{on axis}} \qquad (3-26)$$

The equations used are:

a. Piston radial speed

We can use Eq. (3-18) for this phase by setting put $\left(\frac{dr_s}{dt}\right) = 0$ and $r_s = 0$,

$$\frac{dr_p}{dt} = \frac{-\frac{r_p}{\gamma I}\left(1-\frac{r_s^2}{r_p^2}\right)\frac{dI}{dt} - \frac{r_p}{z_f}\left(1-\frac{r_s^2}{r_p^2}\right)\frac{dz_f}{dt}}{\frac{\gamma-1}{\gamma}+\frac{1r_s^2}{\gamma r_p^2}} \qquad (3-27)$$

b. Pinch elongation speed

This corresponded axial elongation equation in $(3-16)$

c. Circuit Equation

This corresponded circuit equation in $(3-22)$

d: Pinch voltage

This corresponded pinch voltage equation in $(3-24)$.

3.2.4. Slow Compression (Quiescent) or Pinch Phase:

Three coupled equations describe this phase; these being the piston radial motion equation, the pinch column elongation equation and the circuit equation, incorporating the same model parameters as in the

previous two phases. Thermodynamic effects are incorporated into this phase. When the out-going reflected shock hits the in-going piston the compression enters into the radiative phase in which for gases such as neon, radiation emission may actually enhance the compression where we have included energy loss/gain terms from Joule heating and radiation losses into the piston equation of motion.

The duration of this slow compression phase is set as the time of transit of small disturbances across the pinched plasma column. The computation of this phase is terminated at the end of this duration [95].

The equations used are:

a. Radial speed [124]

We can use Eq. (3-18) for this phase by setting $r_s = 0$, $dr_s/dt = 0$,

$$\frac{dr_p}{dt} = \frac{-\frac{r_p dI}{\gamma I dt} - \frac{1}{\gamma+1}\frac{r_p dz_f}{z_f dt} - \frac{4\pi(\gamma-1)}{\mu\gamma}\frac{r_p}{z_f}\frac{dQ}{f_c I^1 dt}}{\frac{\gamma-1}{\gamma}} \qquad (3-28)$$

b. Column elongation [125]

Whereas in the radial RS phase we have adopted a elongation speed model, we now allow the elongation to be driven fully by the plasma pressure.

Eq. (3-28) can be also used to describe the axial elongation in this phase.

$$\frac{dz_f}{dt} = \left[\frac{\mu}{4\pi^2(\gamma+1)\rho_0}\right]^{1/2}\frac{If_c}{r_p} \qquad (3-29)$$

c. Circuit equation

The radial phase circuit equation (Eq. (3-22)) is valid throughout the whole radial phase.

$$\frac{dI}{dt} = \frac{V_0 - \frac{\int Idt}{C_0} - \frac{\mu}{2\pi}\left(\ln\frac{b}{r_p}\right)\frac{dz_f}{dt}If_c + \frac{\mu}{2\pi}\frac{z_f dr_p}{r_p dt}If_c - I(Rf_c + r_0)}{L_0 + \frac{\mu}{2\pi}f_c\left[(\ln c)z_0 + \ln\frac{b}{r_b}\right]z_f} \qquad (3-30)$$

d. Voltage

For Calculate voltage across input terminals of focus tube:

$$V = \frac{\mu f_c}{2\pi} I \left[\left(\ln \frac{b}{r_p} \right) \frac{dz_f}{dt} - \frac{z_f}{r_p} \frac{dr_p}{dt} \right] + \frac{\mu f_c}{2\pi} \left[(\ln c) z_0 + \left(\ln \frac{b}{r_p} \right) z_f \right] \frac{dI}{dt} RI \quad (3-31)$$

Combined with all radial phase equations and expressions, the plasma parameters can be calculated.

The total energy radiated by Bremsstrahlung (Q_B) and line radiation (Q_L) may also be evaluated.

In addition, the radiation energies are calculated as follows:

a. Resistive heating

$$\frac{dQ_J}{dt} = RI^2 f_c^2 \quad (3-32)$$

where $R = \frac{1290 Z z_f}{\pi r_p^2 T^{3/2}}$ is the resistance plasma and I is the current flow.

b. Bremstrahlung loss

$$\frac{dQ_B}{dt} = R - 1.6 \times 10^{-40} N_i^2 \pi r_p^2 z_f T^{1/2} z^3 \quad (3-33)$$

c. Line loss [126]

$$\frac{dQ_L}{dt} = \frac{-4.6 \times 10^{-31} N_i^2 Z Z_n^2 (\pi r_p^2) z_f}{T} \quad (3-34)$$

where N_i number density, Z_e is effective charge number, Z_n is atomic number of gas, r_{pinch} is pinch radius, z_{pinch} is pinch length.

3.2.5. Expanded Column Phase:

In this final phase the snow plow model is used, and two coupled equations are used similar to the axial phase, The snowplow model can be a valuable tool for the study of the PF dynamics and its design optimization, once fixed the external circuit parameters [127]. This phase is not considered important as it occurs after the focus pinch.

The normalized equations for the circuit and the motion are as follows:

a. Circuit equation:

$$\frac{d\iota}{d\tau} = \frac{1-\int \iota d\tau + \beta\iota\frac{d\xi_f}{d\tau}\epsilon - \delta\iota}{1+\beta-\beta(\xi-1)\epsilon} \qquad (3-35)$$

where $\epsilon = (\ln c + 1/z)/\ln c$

b. Motion equation:

$$\frac{d^2\xi}{d\tau^2} = \frac{\left[\alpha^2\iota^2\epsilon_1 - h^2\left(\frac{d\xi}{d\tau}\right)^2\right]}{1+h^2(\xi-1)} \qquad (3-36)$$

where $\epsilon_1 = (\ln c + 1/4)/\ln c$

The initial conditions for ι and $\int \iota d\tau$ are the last values of ι and $\int \iota d\tau$ from the last phase. The initial value of ξ is $\xi = 1 + \xi_f$ where $\xi_f$is the last length of the focus column, but normalised to z_0, rather than a [128,129].

3.3: Studies using the model

The Lee Code has been used to assist several projects [130], and used in the design and interpretation of experiments [131].

It has also been used for various applications, e.g. for estimating soft x-ray yield for the purpose of developing a SXR source for microelectronics lithography [132].

The code has been used extensively in several machines including UNU/ICTP PFF [133, 134], NX2 [135], and NX1 and has been adapted for the Filippov – type plasma focus DENA [136].

The code has been used in numerical experiments to study various plasma focus phenomena [137], such as neutron yields with varying pressure.

It has also been used in other machines for design and interpretation including sub-kJ PF machines.

CHAPTER

FOUR

Results and Discussion

4.1: Introduction

Despite the advantages of scalability for device parameters, the design of plasma focus device is not easy procedure since it involves a number of topics related to the choice of parameters such as the circuit parameters, and the design of the electrode. First of all, we draw the attention on the external circuit parameters and on the design of the electrodes. After that we concentrate on how to use the parameters on Lee code. The input data of disgned plasma focus are introduced in Lee code and the calculations are achieved for two values of pressure. Further comparison with well known NX2 DPF at 4 Torr is carried out. The entire parameters calculations are sketched using Matlab tool due to better fine clarity shown than the original Excel figure and help to make comparison with various cases which is not provided by the original code.

4.2: The electrical parameters

The crude definition of the main electrical parameters is mainly based on macroscopic considerations and experimental observations. The first step in planning of plasma focus is an estimate of the total bank energy and peak current, on the basis of expected operational capacities. Since the charging voltage can be chosen in a very small period of time, the all the other electrical parameters can be extracted easily.

Plasma focus devices are usually operated for very high voltages, higher than those very strictly necessary for the production of gas breakdown. In fact, there is a minimum voltage for the charging of capacitor bank due to the inductive voltage drop during the axial acceleration phase.

It is quite intuitive that the variable induction of the equivalent RLC circuit grows during the sheath motion, since the space occupied by the magnetic field increases with the axial position. Due to the voltage drop related to the inductance element of the circuit by the first term $d(LI)/dt$ of the equation as figure (3.2):

$$\frac{d}{dt}\left[\left(L_0 + L_p(t)\right) I\right] + R_0 I = V_0 - \frac{1}{C_0}\int_0^t I(t')dt' \qquad (4.1)$$

where I is the current, C_0 is the external circuit consists in a capacitor bank, charged at a voltage V_0, connected to the device through an ideal switch; the line presents a total resistance R_0 and a total inductance L_0. During the sheath dynamics, the plasma inductance L_p and its resistance R_p vary in time. The plasma resistance can be usually neglected with respect to the external one.

During the early stages of the discharge, the current grows rapidly, but the induction is mainly due to the external circuit term is constant and order of tens nH. For maximum effect of compression in the focus phase, the current sheath must be accelerated and end in a coincidence of time with the first maximum of the current, since almost given by equation:

$$I(t) = \frac{V_0}{\omega L}\exp(-\xi t)\sin(\omega t) \qquad (4.2)$$

where the typical plasma focus of electrical parameters

$$\xi = \frac{R_0}{2L} \quad \text{and} \quad \omega \simeq \frac{1}{\sqrt{LC_0}} \qquad (4.3)$$

Usually, the plasma focus device equivalent RLC circuit is strongly under – damped, that means $R_0 \ll 2\sqrt{L/C_0}$ with $L = L_0 + L_p$ the total inductance. The typical current waveform of a plasma focus device in short circuit test is exponentially damped sinusoid as in the figure 4.2:

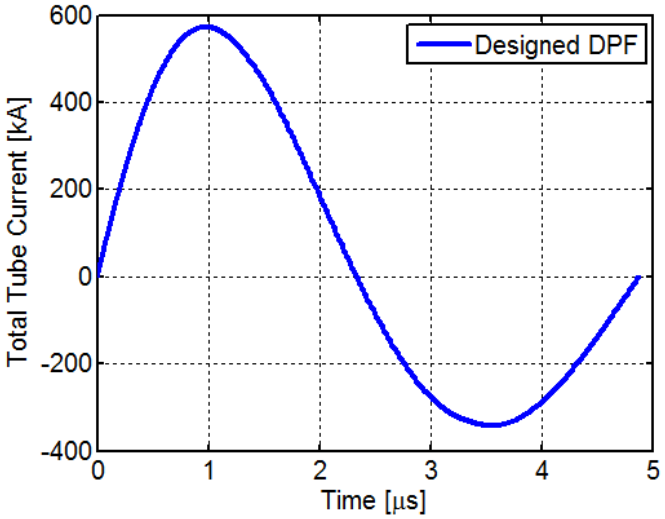

Figure 4.1: Short circuit test of the typical current waveform of a plasma focus device.

It follows that the maximum is given basically the value of the voltage drop by varying component of induction, which means./

$$\frac{d}{dt}[L(t)I(t)] = L\frac{dI}{dt} + I\frac{dL}{dt} \sim I\frac{dL}{dt} \tag{4.4}$$

On this occasion, we can regard the profile of the current sheath in the first approximation with no curvature, and connect the inner electrode radius a with outside electrode of the radius b. Simply apply the formula to calculate the inductance between two coaxial cylinders of length, and induction of the tube focus can be written as

$$L_p(t) = \frac{\mu_0}{2\pi}\ln\left(\frac{b}{a}\right)z(t) \tag{4.5}$$

where $z(t)$ represents the axial position of the current sheath along the electrodes. Inductive voltage drop is, therefore, given by

$$I\frac{dL}{dt} = I(t)\frac{\mu_0}{2\pi}\ln\left(\frac{b}{a}\right)\frac{dz}{dt} \tag{4.6}$$

with $v = dz/\,dt$ macroscopic speed of the sheath during rundown. Usually radii ratio lead to the $\ln(a/b) \simeq 0.5 - 1$, while the peak current

is $I \simeq 0.5 - 1\,\mathrm{MA}$, and this gives the inductive voltage drop in the axial speed

$$\frac{1}{v}dV \simeq \frac{1}{10}\ \mathrm{Vs/m}$$

or, equivalently, about $1\ \mathrm{kV}$ per $1\ \mathrm{cm/\mu s}$.

Range of speeds in the tube axis suitable plasma focus are rather small (4-45): the lower limit is fixed by the efficiency of the electromagnetic drive mechanism. However, usually, it is to take the speed of the current sheath in the range of $3 - 8\ \mathrm{cm/\mu s}$ for tube of plasma focus operating in deuterium. On the other hand, observations also show that it is difficult to get consistent conversion of the axial speed into focusing action when the axial speed exceed $10\ \mathrm{cm/\mu s}$.

It is well known the existence of a minimum operating voltage of the dense plasma focus device, given mainly by the voltage drop across the focus tube during the axial acceleration phase. From the equation (4.6), it follows that the inductive voltage drop tube is in the range of $3 - 10\ \mathrm{kV}$, which is the main reason behind that most of the plasma focus with charging voltages work in the range of $20 - 30\ \mathrm{kV}$. Once fixed the charging voltage V_0, the energy E wanted for the bank imposes the total capacity C_0 of the system, and being

$$E = \frac{1}{2}C_0V_0^2 \qquad (4.7)$$

Immediately after fixing the electrical parameter of the external circle, the precise design of the dimensions of the electrodes must be followed.

4.3: Electrodes Design

To improve the condition of the device is a time coincidence between pinch and the maximum current. Thus, the design of the electrodes is a fundamental aspect: the ratio of radii affects the induction of tube focus, while the total length is linked to the maximum current of the external circuit through the sheath axial velocity.

That a first rough solution have it is coupling the expression of magnetic and gas pressure, given the current sheath of the axial speed by equation

$$v = \sqrt{\frac{\mu_0 I^2}{8\pi^2 \rho r_{int}^2}}$$

Since the speed is proportional to I, consider the $I(t)$ in time of a typical lumped RLC circuit and neglect damping exponential (see equation (1.2)), and the current sheath axial average speed can be obtained on the integration of $I(t)$ over the period of the first quarter and dividing by $\pi/2$:

$$\bar{v} = \sqrt{\frac{\mu_0 \ln\left(\frac{b}{a}\right)}{4\pi^2 \rho (b^2 - a^2)}} \frac{2}{\pi} I_{0,\text{peak}} \int_0^{\pi/(2\omega)} \sin(\omega t) d(\omega t)$$

$$= \sqrt{\frac{\mu_0 \ln\left(\frac{b}{a}\right)}{\pi^4 \rho (b^2 - a^2)}} I_{0,\text{peak}} \qquad (4\text{-}8)$$

where $I_{0,\text{peak}}$ is the maximum ideal current.

Assuming the average rundown velocity as the velocity of the whole phenomenon, the current sheath approaches the end of the electrodes at about

$$t_l = \sqrt{\frac{\pi^4 (b^2 - a^2)}{\mu_0 \ln\left(\frac{b}{a}\right)}} \frac{l \rho^{1/2}}{I_{0,\text{peak}}} \qquad (4 - 9)$$

where l represents the total length of the electrodes.

the period of the sinusoidal current of the equivalent LC circuit (R_0 is here neglected) can be evaluated as

$$T = \frac{2\pi}{\omega} = 2\pi\sqrt{L_0 C_0} \qquad (4 - 10)$$

ω being approximately given by the equations $\omega = \frac{1}{\sqrt{LC_0}}$. The peak current $I_{0,max}$ is reached at time $t_0 = T/4$, which can be compared with current sheath axial transit time of equation (4.9), leading to the scaling parameter

$$\frac{t_l}{t_0} = \frac{1}{2\pi\sqrt{L_0 C_0}} \sqrt{\frac{\pi^4 \rho (b^2 - a^2)}{\mu_0 \ln\left(\frac{b}{a}\right)}} \frac{l}{I_{0,\text{peak}}} \qquad (4-11)$$

$$\simeq \frac{2}{\sqrt{L_0 C_0}} \sqrt{\frac{2\pi^2 a^2 \rho}{\mu_0}} \frac{l}{I_{0,\text{peak}}} \qquad (4-12)$$

for $b/a \lesssim 3$, The ratio should lie around the unity to ensure the maximum transfer of external energy into compression strength.
Another important design parameter is the good matching between the external inductance L_0 the focus tube one L_l

$$\frac{L_l}{L_0} = \frac{1}{L_0} \frac{\mu_0}{2\pi} l \ln\left(\frac{b}{a}\right) \qquad (4-13)$$

In this case, the approaching of the ratio to 1 ensure a good energy transfer from external circuit to magnetic compression. Deviations from the ideal value of 1 could induce the current shedding effect, common to all the type of shock tubes: a portion of the tube current stays behind, near the back-wall insulator sleeve, without contributing to the effective current of the plasma sheath (even if measured by diagnostics).

The two scaling parameters represent a sort of figure of merit (FOM) for the PF design. Typically an error of $\pm 10\%$ on their value can be assumed.

Practically, the two parameters are not enough to set the electrodes geometry. However, experimental data and other theoretical aspects limit the variability range of few variables. As previously shown, current sheath axial speed can vary in a rather small range. Moreover, typical operating pressures are of the order of few Torr to improve gas breakdown and maintain reasonable electrodes dimensions. These limits help in determining an initial trial value for length l and radiuses b and a.

One should notice that the proposed solution needs many refinements. Mainly, no information is yet available on the collapse phase, which is the most critical: the peak current is wanted in time-coincidence of the pinch stage, rather than at the end of the axial transit; moreover, during

the last stages the inductance of the collapsing sheath rapidly increases modifying the peak value and the inductive voltage drop[138,139].

4.4: The procedure to design the new plasma focus

4.4.1: Selection the values of capacitance and inductance

The electrostatic energy is given by equation (4.7). We assume that the bank energy $E = 4.1\,\mathrm{kJ}$, it is convenient to work at high charging voltage to reduce the needed total capacitance.

It follows that at a nominal charging voltage V_0 of $16\,\mathrm{kV}$, the required capacitance is $C_0 = 32\ \mu\mathrm{F}$.

A typical plasma focus peak current I_{peak} is the range $0.2 - 1\,\mathrm{MA}$. From experience, the peak current during focus operation is typically 60% of the maximum ideal current $I_{0,\mathrm{peak}}$. It is therefore necessary to design the external circuit parameter in order to obtain a maximum ideal current $I_{0,\mathrm{peak}} \sim 1.6 - 1.7 I_{\mathrm{peak}}$.

Using $I_{0,\mathrm{peak}} = 1.7 I_{\mathrm{peak}}$ and from equation

$$V_0 = I_{0,\mathrm{peak}} \sqrt{\frac{L_0}{C_0}} \tag{4.14}$$

the total inductance L_0 (here intended as the sum of the external circuit and focus tube inductances) is approximately about $15\,\mathrm{nH}$.

4.4.2: Designing a new plasma focus

Further, we use the simplifying hypothesis that $R_0 \ll 2\sqrt{L_0/C_0}$.

For the stray (circuit) resistance, we use the equation

$$R_0 = \frac{1}{4}\sqrt{\frac{L_0}{C_0}} \tag{4.15}$$

then the stray (circuit) resistance is $5.46\ \mathrm{m\Omega}$, which is satisfies the above hypothesis.

Now to estimate the undamped peak current using the formula

$$I_{\mathrm{peak}} = \frac{V_0}{\sqrt{\frac{L_0}{C_0}}} \tag{4.16}$$

where I_{peak} is 7.3 A

To assign the value of centre electrode radius a we take maximum undamped current per cm and use the equation

$$a = \frac{I_{\text{peak}}}{250\ \text{kA}} \tag{4.17}$$

Then, the centre electrode radius is 2.9 cm

The corresponding value for outer electrode radius b is in double of a, yielding b$= 5.8$ cm

Under the hypothesis $b/a = 2 \leq 3$, a series expansion of the logarithm leads to the approximate relation for length of the electrode to be assigned as 5 times the value of $1.6\sqrt{L_0 C_0}$ .This length is in cm when the value of $\sqrt{L_0 C_0}$ is expressed in microsecond. Therefore the length of the electrode is $z_0 = 5.6$ cm

In our work that the working gas in plasma focus machine is deuterium. The appreciate pressure value to be assign is 4 torr.

To compare whether the designed plasma focus with others we use the ratio of length of electrode to the diameter of the centre electrode to determine whether the designed plasma focus is fat or thin. This ratio is 0.95. From literature the plasma focus of type NX2 this ratio is 1.2 means fat plasma focus; for UNU/ICTP PFF this ratio is 17 means thin.

According to this the designed plasma focus is fat. Therefore the design thumb given by Lee suggested model parameters that used for the NX2 plasma focus. The suggested model parameters are; the axial mass swept – up factor (reduced mass factor due to mass shedding) massf is 0.1, the tube current flow factor (reduced current factor due to current shedding) currf is 0.7 (This value uses for most machines), the radial mass swept – up factor (radial mass factor) massfr is 0.2 and the radial current factor currfr is 0.7 .

To build the model we enter the above assumed and calculated parameters into the appropriate spaces for these machine parameters of Lee code.

Table (4.1): Summarized the input data for the designed plasma focus to be used in Lee code to run the computation:

$L_0 = 15.2$ nH	$C_0 = 23$ μF	$b = 5.8$ cm	$a = 2.9$ cm	$z_0 = 5.6$ cm
$R_0 = 5.46$ mΩ	massf $= 0.1$	cuurf $= 0.7$	massfr $= 0.2$	cuurfr $= 0.7$
$V_0 = 16$ kV	$P_0 = 4$ Torr	MW $= 4$	A $= 1$	mol $= 2$

Running the computation with Lee code we obtain realistic current dip in current profile, indicating good results to be achieved. Furthermore, we reduce working gas pressure to be 3 Torr, and use data of NX2 plasma focus for comparison with the designed plasma focus.

Table (4.2): Summarized the input data for NX2 plasma focus to be used in Lee code to run the computation for comparison:

$L_0 = 20$ nH	$C_0 = 28$ μF	$b = 4.1$ cm	$a = 1.9$ cm	$z_0 = 5$ cm
$R_0 = 2.3$ mΩ	massf $= 0.1$	cuurf $= 0.7$	massfr $= 0.2$	cuurfr $= 0.7$
$V_0 = 11$ kV	$P_0 = 4$ Torr	MW $= 4$	A $= 1$	mol $= 2$

The following sections are a study of the main parameters that affects the work of the design dense plasma focus for two volume of the pressure. The study includes a comparison of the designed dense plasma focus with standard one at the same pressure.

4.5: Current vs. Time

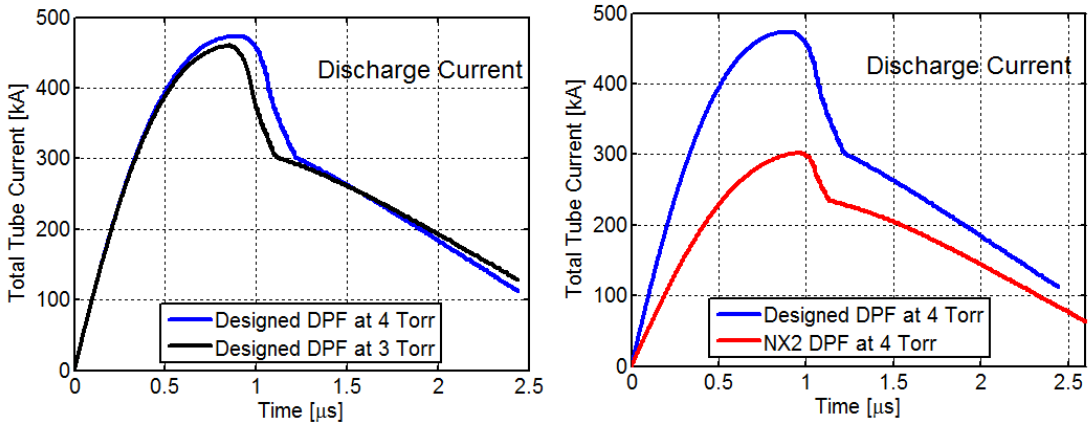

(a) (b)

Fig.(4-3) : (a) Comparison of the current vs. time between designed DPF at 4 Torr and 3 Torr. (b) Comparison of the current vs. time between designed DPF and NX2 DPF at 4 Torr.

Fig .(4-3a) shows the variation of total tube current vs. time for two values of pressure for the designed plasma focus. As mentioned before the plasma focus starts at axial phase. At the end of the axial phase, the current sheath collapse radially and enters the radial phase, and the phase pinch begins. It is noted that the current dip of designed plasma focus at $3\ torr$ agrees with current dip at $4\ torr$. The realistic current dips in current profile shown in figure, indicating good results for the designed plasma focus. Further, it is noted that the overall computed discharge current waveform of designed plasma focus agrees at $3\ torr$ well with most the $4\ torr$ current waveform. The exact time profile of the total current trace is governed by the bank parameters, by the focus tube geometry and the operational parameters.

The two curves of current profile coincide at the early time or current rise slope and they are away from each other just before reaching to the topping profile. However, the peak value of the current

for lower pressure is less than higher and the slope of current dip starts and finishes at advance time. It is noted that the bottom of the current dip starts early for lower pressure than the higher one. At the end of the pinch phase the total current profile also reflects the sudden transition of the current flow from a constricted pinch to a large column flow. The effect of lowering the pressure is to lower the current profile. While the peak current value for a pressure $4\ \mathrm{Torr}$ is about $473\mathrm{A}$ at time $0.851\mu s$, it's $460\mathrm{A}$ at the time $0.842\mu s$ for a pressure $3\ \mathrm{Torr}$. For the pressure $4\ \mathrm{Torr}$ the time of radial starts at $0.915\mu s$ and ends at time$1.22\mu s$. Thus the radial duration is $0.305\mu s$. For the pressure $3\ \mathrm{Torr}$ the time of radial starts at $0.842\mu s$ and ends at time $1.11\mu s$. Thus the radial duration is $0.268\mu s$. The computed pinch duration of designed plasma focus at pressure $4\ \mathrm{Torr}$ is $48.555\ \mathrm{ns}$ while it's $42.164\ \mathrm{ns}$ at pressure of $3\ \mathrm{Torr}$. Therefore increasing the pressure leads to increase the radial and pinch duration.

Fig. (4-3b) shows the variation of total tube current vs. time between designed DPF and NX2 DPF at $4\ \mathrm{Torr}$. It is clear that the designed plasma focus has higher current profile than NX2 DPF due to differences in geometrical design of both plasma focus machines. Further the current dip in the designed plasma focus last more time than NX2 DPF. It noted that the bank energy E_0 of NX2 DPF is lower than the designed plasma focus therefore the peak current of designed plasma focus is higher than that of NX2 DPF. For the pressure $4\ \mathrm{Torr}$ of NX2 DPF the time of radial starts at $0.947\mu s$ and ends at time $1.135\mu s$. Thus the radial duration is $0.187\mu s$. The computed pinch duration of NX2 DPF is $27.043\ \mathrm{ns}$. Thus the pinch duration of designed plasma focus is higher than NX2 DPF. Moreover, the radial duration of NX2 DPF is lower than the designed plasma focus at the same pressure.

4.6: Voltage vs. Time

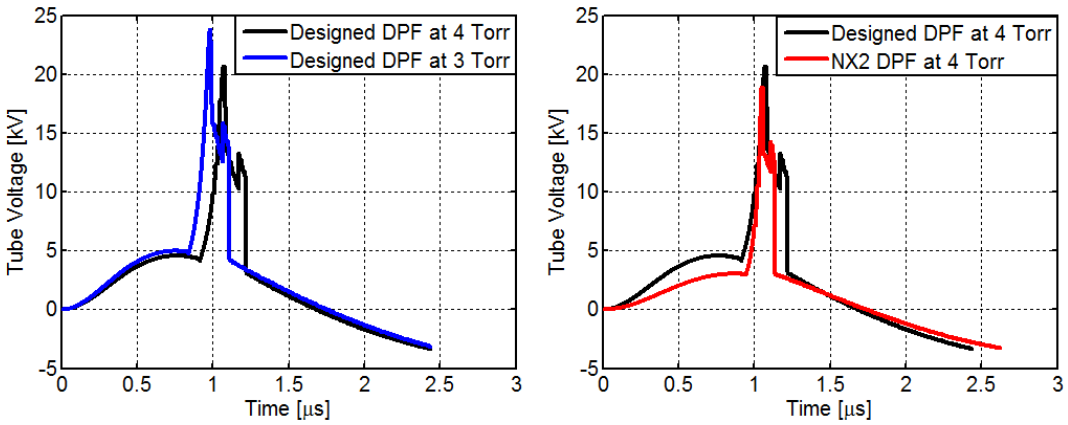

(a) (b)

Fig.(4-4): (a) The tube voltage vs. time for the designed DPF at 4 Torr and 3 Torr. (b) The tube voltage vs. time for the designed DPF and NX2 DPF at 4 Torr.

Fig. (4-4a) shows the variation of tube voltage vs. time for two values of pressure. It is noted that the start of voltage waveform peak is the end of axial phase and a start of radial pinch phase. Note that the peak value of the tube voltage at pressure 4 Torr is 20.7 kV at time 0.107μs and at pressure 3 Torr the peak value of the tube voltage is 23.8 kV at time is 0.984μs . Thus decreasing the pressure is to raise the peak voltage that grows in advance time. The spikes voltages follow the peak voltage for both pressures till the sharp decline indicating the pinch phase. The spike voltage at 3 Torr is as expected to be sharper, higher and with larger amplitude than that at 4 Torr. Comprehensibility, at low pressure 3 Torr the voltage has too fast drop from peak voltage due to the moving radial phase into the expanded column phase. The higher voltage spikes and deeper current dip could result in better focusing conditions.

Fig. (4-4b) shows the variation of tube voltage vs. time between designed DPF and NX2 DPF at 4 Torr. The two curves of both machines at the same pressure are coinciding well. However, the evolution of the designed plasma focus be tougher and has amplitude greater than the NX2 DPF curve. The reason for this can be attributed to the difference in the geometric electrodes between the two systems.

4.7: The Axial Speed vs. Time

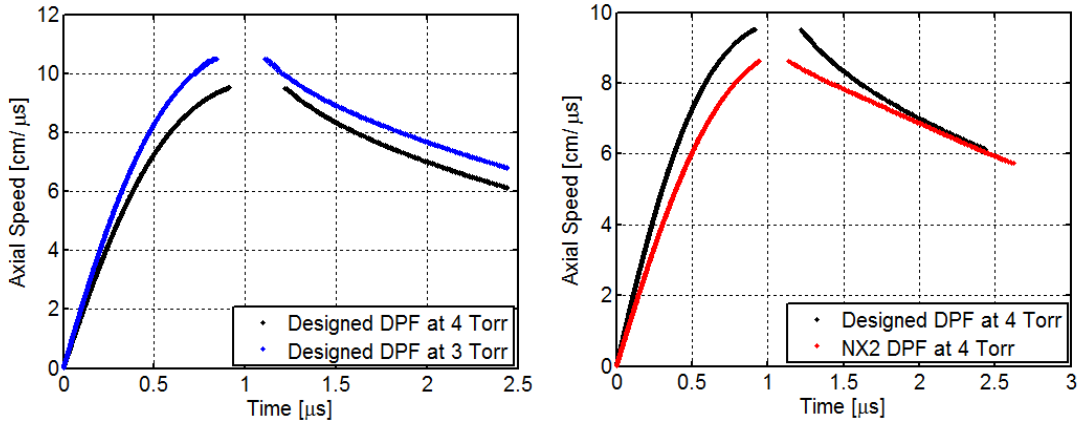

(a) (b)

Fig.(4-5): (a) The axial speed vs. time for the designed DPF at 4 Torr and 3 Torr. (b) The axial speed vs. time for the designed DPF and NX2 DPF at 4 Torr.

Fig. (4-5a) shows the variation of the axial speed vs. time for a couple of gas pressures. Clearly the axial speed increase gradually and slightly continues toward its speed peak at the end of the axial phase. The speed of the current sheath reaches the end of the axial phase at 3 Torr is faster than a peak speed at 4 Torr. Thus the computed current dip (in figure 5.1a) comes much too early because the high speed would also lower the peak current shift of the current dip that comes earlier at lower pressures is consistent with higher axial speeds.

The axial speed increases to its peak value $9.52\ \mathrm{cm/\mu s}$ at time $0.915\mu s$ for pressure 4 Torr and $10.5\ \mathrm{cm/\mu s}$ at time $0.842\mu s$ for pressure 3 Torr. Thus, at 3 Torr the axial speed is so high that the axial phase is completed in less than $0.842\mu s$ and the current (in figure 5.1a) is still rising when it is forced down by the radial phase dynamics. When the last works the code stop to compute the speed till finishing the pinch phase and starts to compute the speed. The axial speed drops or deflected slightly at the end pinch phase with speed $9.50\ \mathrm{cm/\mu s}$ at $1.22\mu s$ for pressure 4 Torr and for pressure 3 Torr that the speed is $10.5\ \mathrm{cm/\mu s}$ at $1.11\mu s$. As the pressure is increased the axial speed decreased, hence, the duration of the axial phase increases.

Fig. (4-5b) shows the variation of the axial speed vs. time between designed DPF and NX2 DPF at 4 Torr. This figure shows that the computed axial speed of the designed plasma focus agrees with standard axial speed of NX2 DPF at the same pressure but the computed axial speed of the designed plasma focus is lower than for standard NX2 DPF.

4.8: The Axial Position Trajectory vs. Time

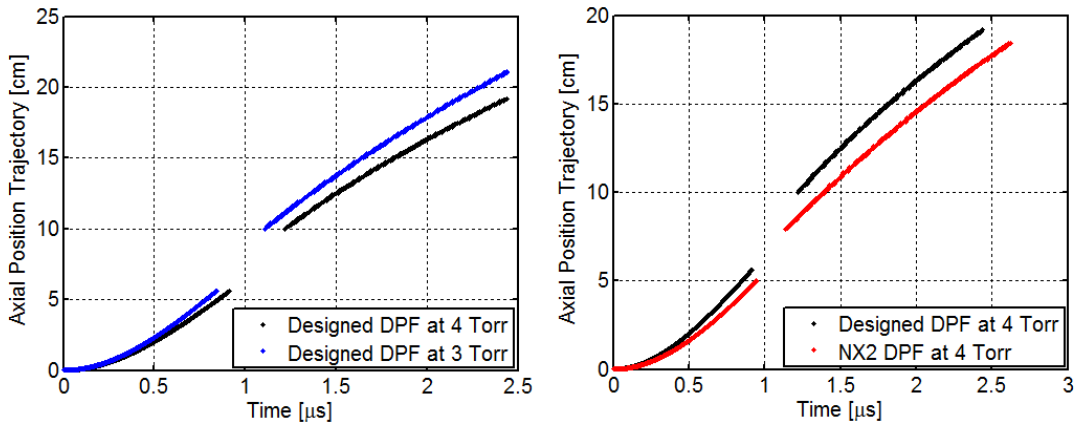

(a) (b)

Fig.(4-6): (a) The axial position trajectory vs. time for the designed DPF at 4 Torr and 3 Torr. (b) The axial position trajectory vs. time for the designed DPF and NX2 DPF at 4 Torr.

Fig. (4-6a) shows the variation of the axial position trajectory vs. time for different gas pressures. As the time increases the axial position continue to rise and reach the value 5.61 cm before the cut off at 0.915 μs for pressure 4 Torr and to the same position 5.61 cm at time 0.842 μs before the cut off for pressure 3 Torr. Note that duration at 4 Torr longer than the duration at 3 Torr. After the cut off the axial position continue rise towards the end pinch phase at position 10 cm at time 1.22 μs for pressure 4 Torr. And for pressure 3 Torr the axial position starts to increase from the same position but early time that is 1.11 μs. Since the same curves of axial positions of the plasma for various pressures the higher pressure results in the plasma last higher time in the axial position.

Fig. (4-6b) shows the variation comparison of the axial position trajectory vs. time between designed DPF and NX2 DPF at 4 Torr. This

figure shows the axial position trajectory is in well agreement for both the designed and the standard plasma focus. Also the behavior is consistent with the pressure of both the designed and the standard plasma focus but the standard one last more time before and after the cut off than the designed. The axial position trajectory cuts off in 5.01 cm at time 0.947 μs. After the cut off it starts at early time 1.14 μs at position 7.91 cm.

4.9: The Radial Inward Shock Trajectory vs. Time

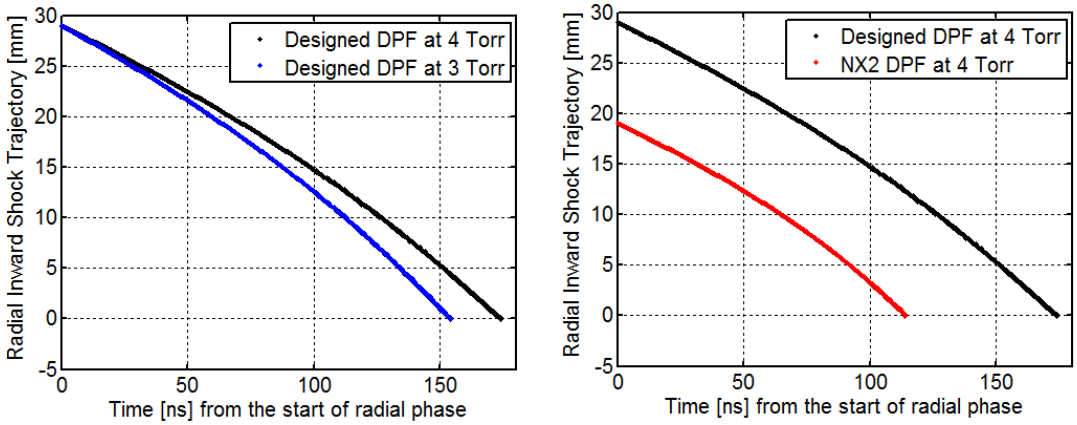

(a) (b)

Fig.(4-7):(a) The radial inward shock trajectory (radial position of shock) vs. time for the designed DPF at 4 Torr and 3 Torr. (b) The radial inward shock trajectory (radial position of shock) vs. time for the designed DPF and NX2 DPF at 4 Torr.

Fig.(4-7a) shows the variation of radial inward shock trajectory vs. time for different pressures. The inward shock trajectory curve is decreased from same point 29 mm till 0 mm for two values of gas pressures used. The duration is 174 ns for a pressure 4 Torr and 154 ns for a pressure 3 Torr. Thus the radial inward shock trajectory at lower gas pressure suffers shorter duration than higher pressure because of the internal reflections. As the time progress forward the radial inward shock trajectory gets diminished. At this time the pinch starts and the column compresses inwards.

Fig.(4-7b) shows the variation of the radial inward shock trajectory vs. time between designed DPF and NX2 DPF at 4 Torr. This figure

illustrates the approval of the trajectories of both the standard with the designed plasma focus. Moreover, the behavior is well consistent with the pressure between two machines. The radial position of shock of the designed plasma focus is higher and takes greater period of time from the standard one. This is due to the increased length of the anode and decreasing radius of designed plasma focus. The inward shock trajectory curve for standard plasma focus is decreased from point $19\ \text{mm}$ and vanished at $0\ \text{mm}$ at the value of gas pressure used. The duration is last $114\ \text{ns}$.

4.10: The Radial Piston Trajectory vs. Time

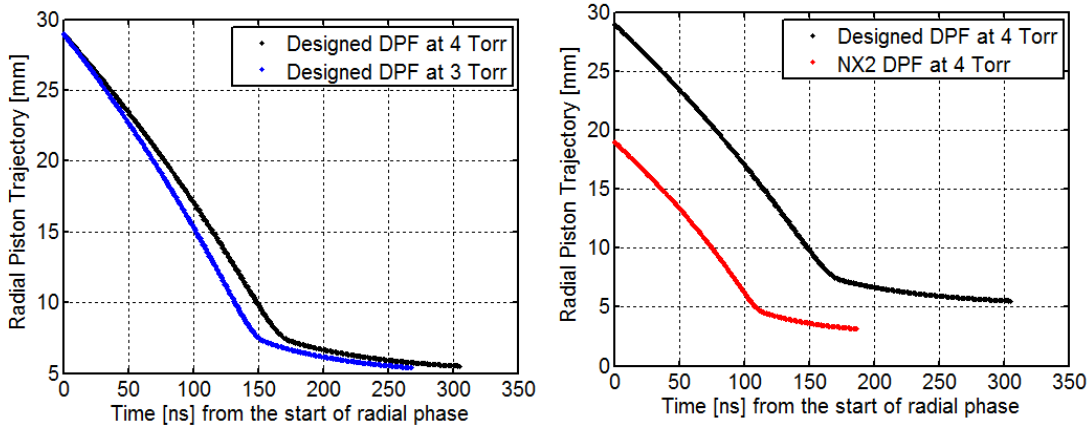

(a) (b)

Fig.(4-8): (a) The radial piston trajectory (radial position of the piston) vs. time for the designed DPF at $4\ \text{Torr}$ and $3\ \text{Torr}$. (b) The radial piston trajectory (radial position of the piston) vs. time for the designed DPF and NX2 DPF at $4\ \text{Torr}$.

Fig.(4-8a) shows the variation of radial piston trajectory vs. time for two values of pressures. As time advances the radial piston sharply falls down reaching to time point such that it linearly decreased. The radial piston trajectory decline from the same point $29\ \text{mm}$ for the both values of pressure and as the time passage it's sharply fall down. The duration of radial piston trajectory for a pressure $4\ \text{Torr}$ is $305\ \text{ns}$, while it's $267\ \text{ns}$ for $3\ \text{Torr}$. Thus as the pressure decreases the radial piston trajectory decreased.

Fig.(4-8b) shows the variation of the radial inward shock trajectory vs. time between designed DPF and NX2 DPF at 4 Torr. This figure shows that the radial piston trajectory of the designed plasma focus agrees well with the standard but trails designed plasma focus. However, the entire values of radial inward shock trajectory of designed plasma focus are higher than the standard due to the electrical specifications of both machines. The radial inward shock trajectory of NX2 DPF at 4 Torr starts at 19 mm and finished at 3.15 mm with duration of 187 ns . This means that the duration of inward shock trajectory of NX2 DPF at 4 Torr is lower than the designed plasma focus at same pressure and even for 3 Torr.

4.11: The Pinch Elongation Trajectory vs. Time

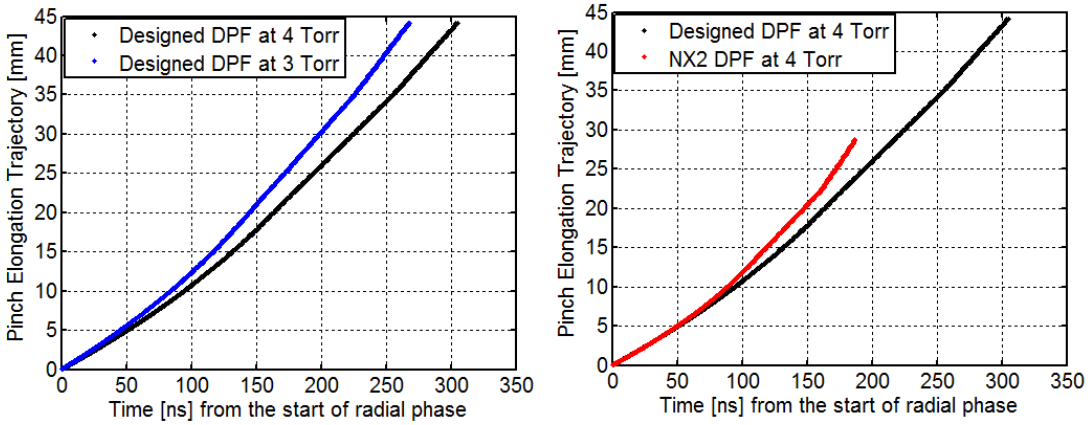

(a) (b)

Fig.(4-9) : (a) The pinch elongation trajectory (radial position of focus length) vs. time for the designed DPF at 4 Torr and 3 Torr. (b) The pinch elongation trajectory (radial position of focus length) vs. time for the designed DPF and NX2 DPF at 4 Torr.

Fig.(4-9a) shows the variation of pinch elongation trajectory with time for two values of pressure. The behavior of the pinch elongation trajectory at 4 Torr in above figure is similar to the pinch elongation trajectory at 3 Torr for the designed DPF, however the maximum of pinch elongation at 4 Torr is the same as pinch elongation trajectory at 3 Torr even that it lasts longer duration as the pressure increased.

Therefore the effect of the pressure is to delay the pinch elongation trajectory of the machine.

Fig.(4-9b) shows the comparison of pinch elongation trajectory for the standard and designed DPF at the same pressure. The pinch elongation trajectory for both devices increases exponentially with time. However, the pinch elongation trajectory for the designed dense plasma is longer than the standard one since it lasts more time. The pinch elongation trajectory for standard dense plasma is lower than 30 mm while the designed one reaches to a value up to 44 mm. The reason behind that is due to the parameters of the tube. Obviously from the figure they coincide at the early time and then they separated as time pass. The behavior of designed dense plasma focus is in good agreement with standard one.

4.12: The Radial Reflected Shock Trajectory vs. Time

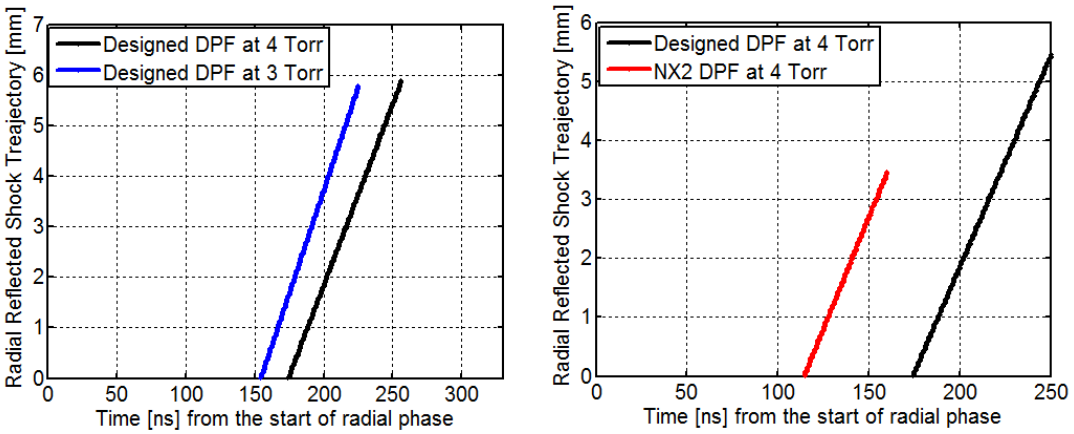

(a) (b)

Fig.(4-10): (a) The radial reflected shock trajectory vs. time for the designed DPF at 4 Torr and 3 Torr. (b) The radial reflected shock trajectory vs. time for the designed DPF and NX2 DPF at 4 Torr.

Fig.(4-10a) exhibits the variation of radial reflected shock trajectory with time for two values of pressures. The computed radial reflected shock trajectory of designed dense plasma shows a steady linearly increase for both values of pressure in the radial phase time. But we note that the radial reflected shock trajectory at 3 Torr begins at time shorter than the radial reflected shock trajectory at 4 Torr. Hence

the radial reflected shock trajectory delays with higher pressures value. Also we note as the pressure increased the radial reflected shock trajectory is longer than lower pressure. It is 5.88 mm for a pressure 4 Torr while it is 5.97 mm for the pressure 3 Torr.

Fig.(4-10b) reveals the comparison of the radial reflected shock trajectory at same pressure for the designed and NX2 DPF. The behavior of radial reflected shock trajectory for designed DPF is similar to the NX2 at 4 Torr. Our designed DPF fits well with the NX2 DPF results. But the radial reflected shock trajectory of the designed DPF is longer than the value of the NX2 increases, and in radial time it is start after. It starts at 115 ns for NX2 DPF whereas it starts 174 ns for the designed dense plasma. The radial reflected shock trajectory of NX2 DPF is shorter than the designed one.

4.13: The Radial Shock Speed vs. Time

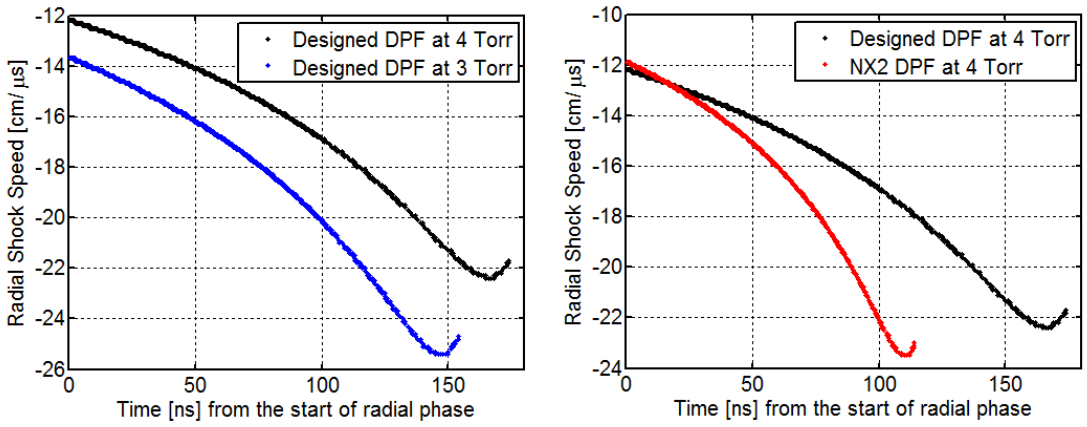

(a) (b)

Fig.(4-11): (a) The radial shock speed vs. time for the designed DPF at 4 Torr and 3 Torr. (b) The radial shock speed vs. time for the designed DPF and NX2 DPF at 4 Torr.

Fig.(4-11a) shows up the variation of the speed radial shock vs. time from the start of radial phase for two different values of pressure. The curves of the radial shock speed decreased exponentially in negative sign reaching to peak and then slightly increase for fixed value. The value of the shock speed for the designed at pressure 4 Torr are higher than

the shock speed at pressure 3 Torr. This means that when the operating pressure increased, the plasma speeds decrease in negative sign, hence, the duration of the radial phase increases.

It appears from Fig.(4-11b) the general agreement between our designed PDF curve and the NX2 curves. The two curves at the same pressure but the NX2 dense plasma focus starts at higher radial shock speed in negative sign and completed at period lower than the designed plasma focus. The NX2 curve at 4 Torr has a minimum at inflection point$(112\ \text{ns}, -23.5\ \text{cm}/\mu\text{s})$ before increased, while the designed dense plasma has a minimum at infection point $(168\ \text{ns}, -22.4\ \text{cm}/\mu\text{s})$. The drop – off of the speed at the same pressure is very similar, but the designed plasma focus has drop – off sharper than the drop – off of NX2 PDF.

4.14: The Radial Piston Speed vs. Time

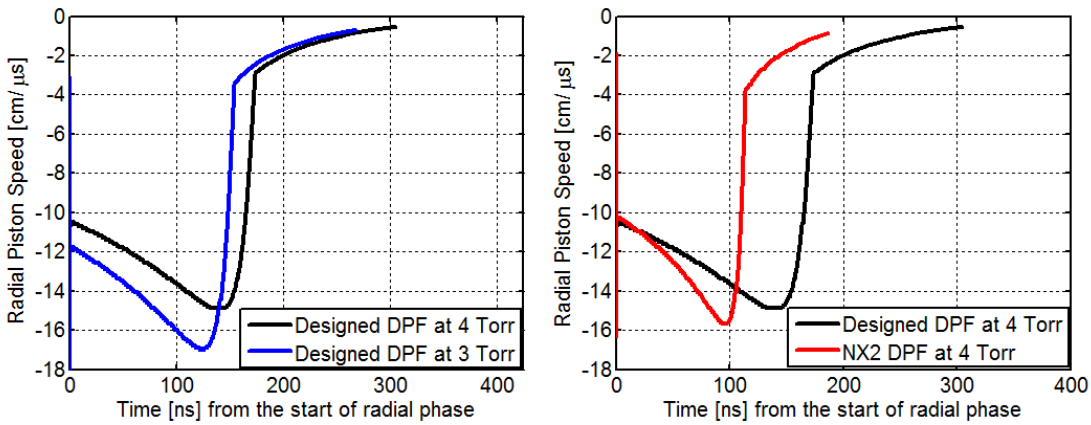

(a) (b)

Fig.(4-12): (a) The radial piston speed vs. time for the designed DPF at 4 Torr and 3 Torr. (b) The radial piston speed vs. time for the designed DPF and NX2 DPF at 4 Torr.

Fig.(4-12a) shows the variation of radial piston (current sheath) speed versus time for different two values of gas pressure. It clear from the figure that the current sheath speed decreases and then increases in a fashion way. The current sheath speed decreases until a minimum point of inflection followed by steadily sharp increased in short time and then reaching to a certain point followed by slowly increases with

relative longer time from the start of radial phase. As the pressure increases the fashion of curve is higher in speed expect the latter stage of increasing. It is well known, when the operating pressure is increased, the plasma speeds decrease; hence, the duration of the axial phase increases. As expected as pressure is increased, the radial piston speed reduced.

Fig.(4-12b) the comparison shows that both the results are in good agreement. However, the current sheath speed starts from nearly the same point and decrease to the point of infection but it takes short time for the NX2 PDF. Generally the current sheath speed of the NX2 PDF tends to shift to lift than designed PDF which means that the current sheath speed has shorter time from the start of radial phase. The current sheath speed of the two devices in the radial phase has radially imploding shock front goes on axis.

4.15: The Pinch Elongation Speed vs. Time

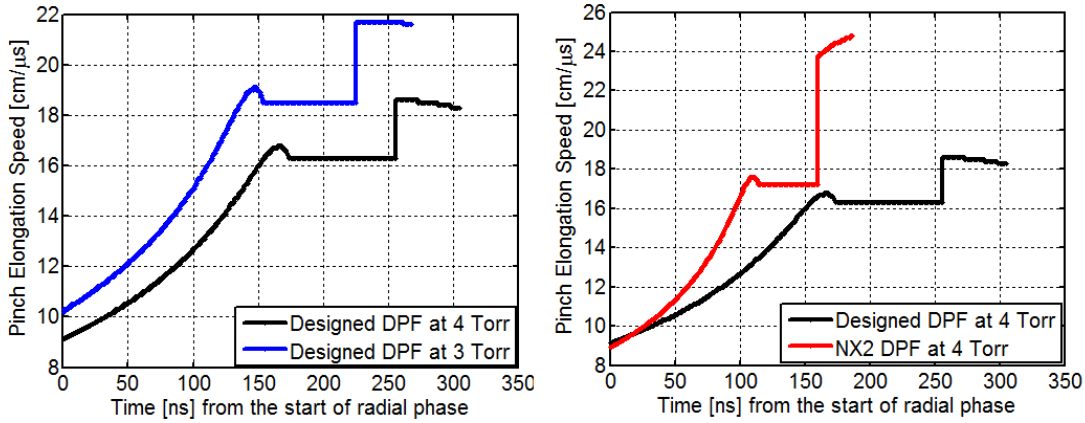

(a) (b)

Fig.(4-13): (a) The pinch elongation speed (axial elongation speed) vs. time for the designed DPF at 4 Torr and 3 Torr. (b) The pinch elongation speed (axial elongation speed) vs. time for the designed DPF and NX2 DPF at 4 Torr.

Fig.(4-13a) shows the variation of pinch elongation speed versus time for two different values of gas pressure. Obviously the curve of pinch elongation speed at pressure 3 Torr is shifted higher than the pressure at 4 Torr. The curve of pinch elongation speed increases

exponentially to a maximum point followed by decreasing in very short time until a point with no acceleration and then increases in fixed value and later decreases at step again with no acceleration. The reason of this behavior is that the axial shock is propagated in the z - direction, towards the downstream anode axis.

Fig.(4-13b) shows the comparison of both the designed DPF and NX2 DPF at the same pressure for pinch elongation speed. It is notice that the pinch elongation speeds for both machines started nearly from the same point and increased exponentially. The pinch elongation speed of designed DPF reaches up to $16.8\ \mathrm{cm/\mu s}$ at time $165\ \mathrm{ns}$ while the NX2 DPF up to $17.6\ \mathrm{cm/\mu s}$ at time $108\ \mathrm{ns}$ from the start of radial phase. This means that the slope of designed DPF is lower than that for NX2 DPF at same pressure. The higher value of the pinch elongation speed for the designed can be explained by the dependence it's on the plasma temperature or anode length (parameters of the tube).

4.16: The Tube Current vs. Time

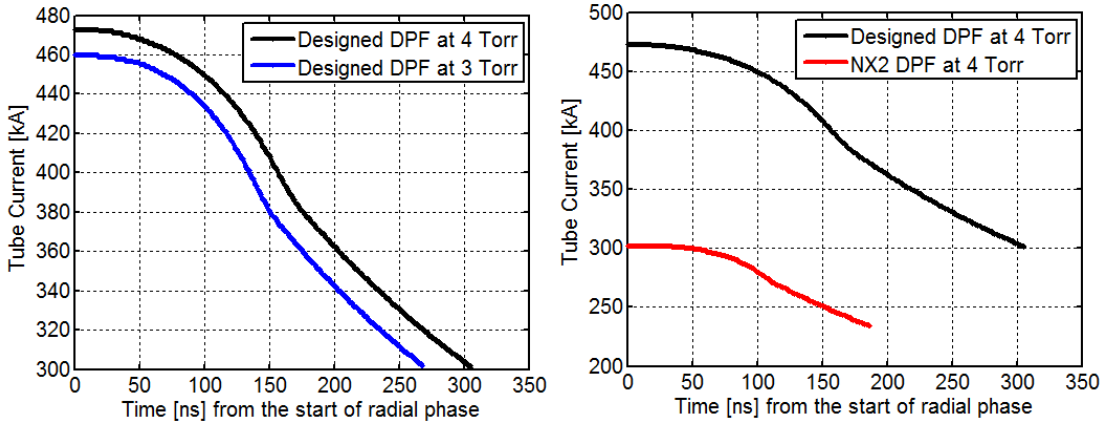

(a) (b)

Fig.(4-14): (a) The tube current vs. time for the designed DPF at 4 Torr and 3 Torr. (b) The tube current vs. time for the designed DPF and NX2 DPF at 4 Torr.

Fig.(4-14a) shows the variation of tube current vs. time for designed PDF at a pressure $4\ \mathrm{Torr}$ and $3\ \mathrm{Torr}$. The curves decrease exponentially and then linearly decreased. As the pressure increases the profile of the curve is higher. The current drop at $4\ \mathrm{Torr}$ and $3\ \mathrm{Torr}$ is

induced by the sharp increase of inductance and resistance of plasma in the radial phase during which the plasma is compressed to a small column. Just before the current drops from peak value I_{peak} and then again near the bottom of the almost linear drop to I_{pinch}.

Fig.(4-14b) shows the variation of designed and NX2 PDF current tube vs. time from the start of radial phase. The NX2 PDF plasma current tube shows good agreement of with the designed PDF. Note that NX2 PDF current tube starts at $300\,\mathrm{kA}$ while the designed PDF start at $437\,\mathrm{kA}$. The behavior depends on three ratios that are the characteristic times, inductances and impedances.

4.17: The Tube Voltage vs. Time

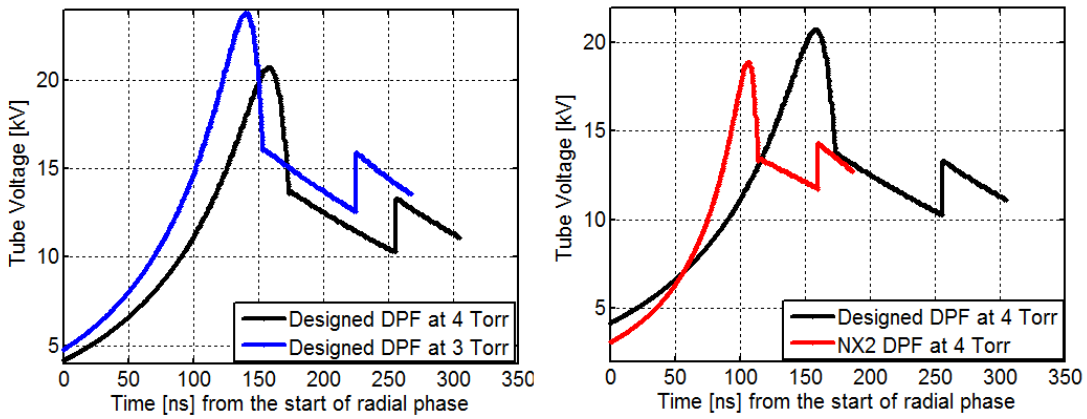

(a) (b)

Fig.(4-15): (a) The tube voltage vs. time for the designed DPF at 4 Torr and 3 Torr. (b) The tube voltage vs. time for the designed DPF and NX2 DPF at 4 Torr.

In Fig.(4-15a) displays the waveform of the tube voltage vs. time from the start of radial phase for the designed DPF at a pressure $4\,\mathrm{Torr}$ and $3\,\mathrm{Torr}$. Note the peak value of the tube voltage is induced by the rapid plasma motion. The peak of waveform of the tube voltage increases as the pressure decreased. The waveform increases exponentially reaching to a maximum value and then linearly falls down with a linearly rise until damping. The tube voltage pulse drops to a value of $14\,\mathrm{kV}$ at pressure $4\,\mathrm{Torr}$, and to $16\,\mathrm{kV}$ at pressure $3\,\mathrm{Torr}$. And the end of the waveform the tube voltage is slightly above $10\,\mathrm{kV}$ at pressure

4 Torr and 13 kV at pressure 3 Torr. The two waveforms of tube voltage are similar. The peak of waveform for higher pressure is smaller than the lower pressure and it occurs with long period of time. This means that at low pressure case it comes too fast due to the instantaneously moving radial phase into the expanded column phase. Accordingly, the effect of the pressure on the tube voltage waveform is to delay the rise time and advancement.

Fig.(4-15b) shows the variation of waveform for the tube voltage vs. time from the start of radial phase for the designed DPF and NX2 PDF at 4 Torr. Even the both waveforms are identical but it clear that NX2 PDF takes short time than the designed PDF. The voltage waveforms depend on the tool circuit of both machines.

4.18: The Plasma Temperature vs. Time

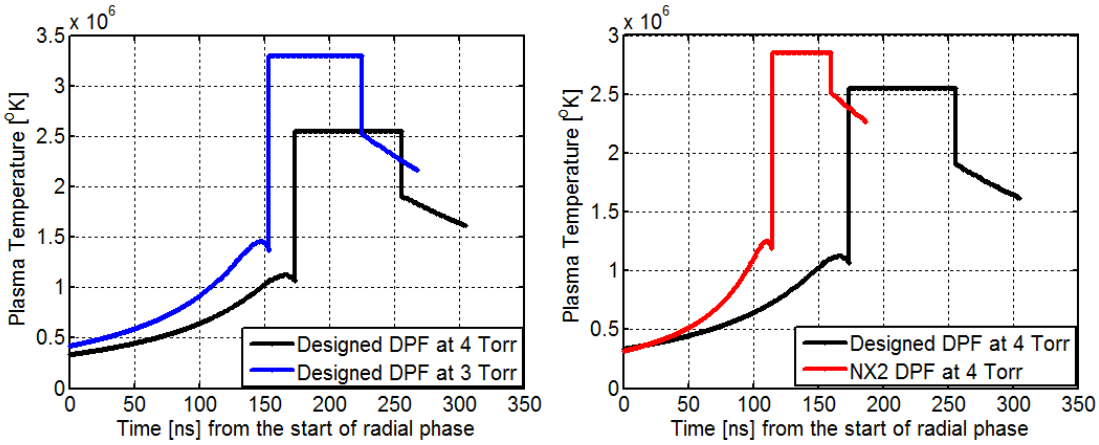

Fig.(4-16): (a) The plasma temperature vs. time for the designed DPF at 4 Torr and 3 Torr. (b) The plasma temperature vs. time for the designed DPF and NX2 DPF at 4 Torr.

Fig.(4-16a) shows the variation of the plasma temperature vs. time from the start of radial phase for two values different pressure. The curves of the plasma temperature at *4* Torr are similar to the curves of the plasma temperature at *3* Torr but as the pressure decreases the profile of the plasma temperature rises up. The curves show early exponential increased of the plasma temperature until a critical point whereas it's sharply increases with a rectangle shape and then linearly

decreased. The plateau part in the upper side of both temperature curves is due to a constant shock speed. The plasma temperature depends on the shock wave velocity due to the lower value of the shock wave velocity in the designed at 4 Torr to 3 Torr. Hence the decrement of plasma temperature after that is due to the lower discharge current hence lower input energy.

Fig.(4-16b) presents the comparison of the NX2 DPF and designed DPF of the plasma temperature. Comparing designed versus time with the NX2 DPF shows general agreement between the designed curve and the NX2 DPF curve. But the designed curve profile shows that the plasma temperature at 4 Torr is to be lower than that for the NX2 DPF and takes longer time than NX2 DPF.

4.19: The Joule Heat vs. Time

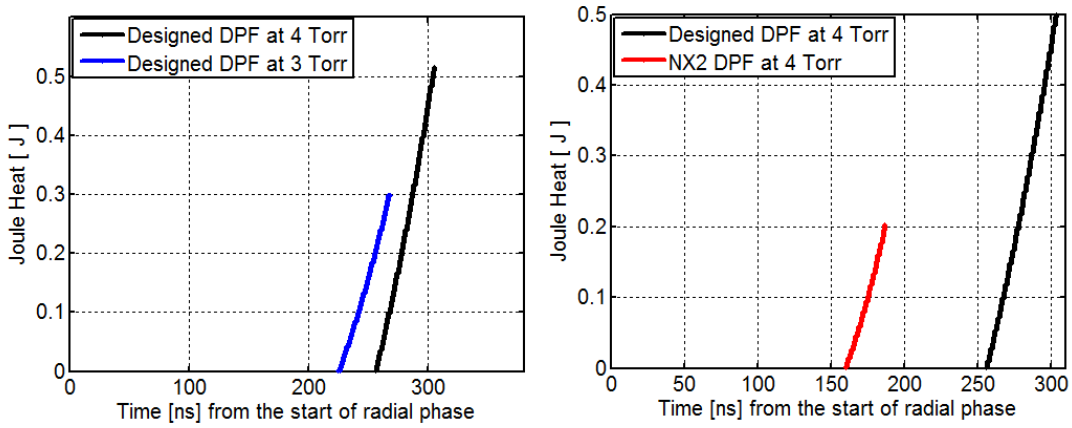

(a) (b)

Fig.(4-17): (a) Joule Heat (resistive Heat) vs. time for the designed DPF at 4 Torr and 3 Torr. (b) Joule Heat (resistive Heat) vs. time for the designed DPF and NX2 DPF at 4 Torr.

Fig.(4-17a) shows Joule Heat (resistive Heat) vs. time for the designed DPF at a pressure of 4 Torr and 3 Torr. Joule heating is the process by which the passage of an electric current through a conductor releases heat. The joule heating is induced by the plasma resistance and the flow of current through it. It directly heats the plasma. The maximum joule heat point at 4 Torr is 0.515 J while at 3 Torr

is 0.3 J. The joule heat value grows at 4 Torr later in time from the start of radial phase than at 3 Torr. The joule heat value increase as the pressure increases. This can describe the very small values of joule heat at lower pressure where the values of pressure are small due to small values of joule heat.

Fig.(4-17b) shows the variation of Joule Heat vs. the time from the start of radial phase for the designed DPF and NX2 DPF at 4 Torr. In fact the absolute value of Joule Heat for the designed DPF is higher than the NX2 DPF. The designed DPF is higher due to lower temperature or the difference in geometrical parameters.

4.20: The Bremsstrahlung Energy vs. Time

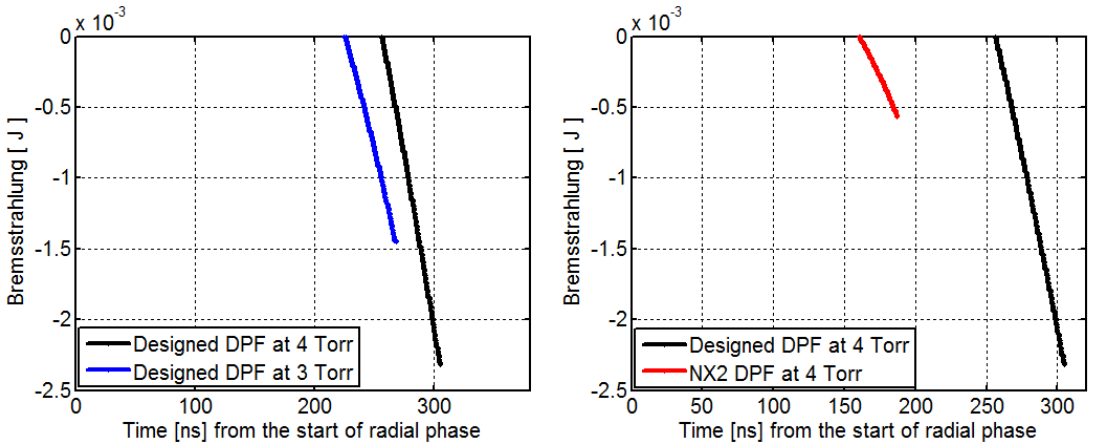

Fig.(4-18): (a) Bremsstrahlung energy vs. time for the designed DPF at 4 Torr and 3 Torr. (b) Bremsstrahlung energy vs. time for the designed DPF and NX2 DPF at 4 Torr.

Fig.(4-18a) shows the variation of the Bremsstrahlung energy vs. time from the start of radial phase for two different pressure values. We define Bremsstrahlung, German word for braking radiation as the radiation emitted by a moving charged particle accelerated by collisions with other particles. Because a particle's acceleration is inversely proportional to its mass for a given force, the Bremsstrahlung emitted by ions is much less than that of electrons. Bremsstrahlung can be emitted through a process known as a "free-free" transition of an electron. In this process, a free electron is deflected by Coulomb forces due to other

charged particles in its vicinity [140]. As can be seen from the figure that as the pressure increased (4 Torr) lead to a higher Bremsstrahlung irradiation with time.

Fig.(4-18b) shows the comparison between Bremsstrahlung energy vs. time for the designed DPF and NX2 DPF at 4 Torr. We see that the designed dense plasma focus has more Bremsstrahlung energy loss than NX2 DPF due to designed engineering specifications.

4.21: The Recombination Energy vs. Time

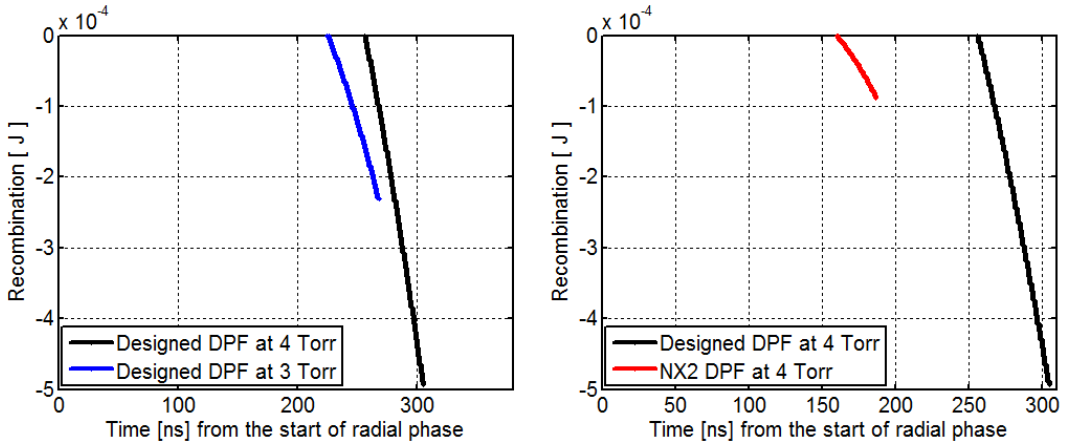

(a) (b)

Fig.(4-19): (a) Recombination energy vs. time for the designed DPF at 4 Torr and 3 Torr. (b) Recombination energy vs. time for the designed DPF and NX2 DPF at 4 Torr.

Fig.(4-19a) shows the variation of the recombination energy vs. time from the start of radial phase for the two different pressure values. A Free electron can be captured into a bound state of an ion, thereby reducing the ionic charge by unity which is emitted by an initially free electron as it loses energy on recombination with an ion [141]. Any excess energy of electron may be emitted recombination radiation. It decreases to negative sign at different pressure values. It clear from the figure, the recombination energy is linear as temperature increases and time from the start of radial phase.

Fig.(4-19b) shows that the recombination energy vs. time from the start of radial phase for the standard DPF NX2 and designed DPF at same

value of pressure. It clear that the value of recombination energy of standard DPF NX2 is small compared to the design DPF.

4.22: The Line Radiation Energy vs. Time

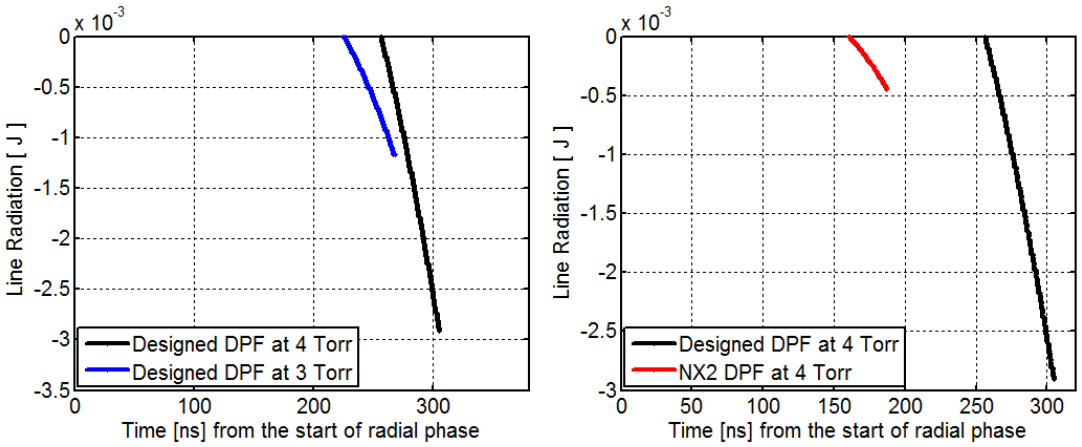

(a) (b)

Fig.(4-20): (a) Line radiation energy vs. time for the designed DPF at 4 Torr and 3 Torr. (b) Line radiation energy vs. time for the designed DPF and NX2 DPF at 4 Torr.

Fig.(4-20a) shows the variation of the Line radiation energy vs. time for the two different pressure values. When an ion, an atom or a molecule is in the excited state, it will undergo a transition to the ground state through spontaneous or simulated emission. Since the energy levels inside the atom are quantified, this emission appears as a discrete packet of energy or lines[141]. The diagrams are similar of both value of the pressure 4 Torr and 3 Torr for the line radiation energy. They have exponentially decreasing. It is clear that for certain value of the line radiation energy decreases towards lower temperature. The line radiation energy decrease as the electron temperature decreases as one can expect. However, the line radiation energy decreases when the pressure decrease. This is because of the radiation loss varies with pressure.

Fig.(4-20b) shows the line radiation energy for same values of pressure for designed and NX2 DPF. They have different maximum

values. The maximum of the line radiation energy designed DPF is shifted towards higher time from the start of radial phase.

4.23: The Specific Heat Ratio vs. Time

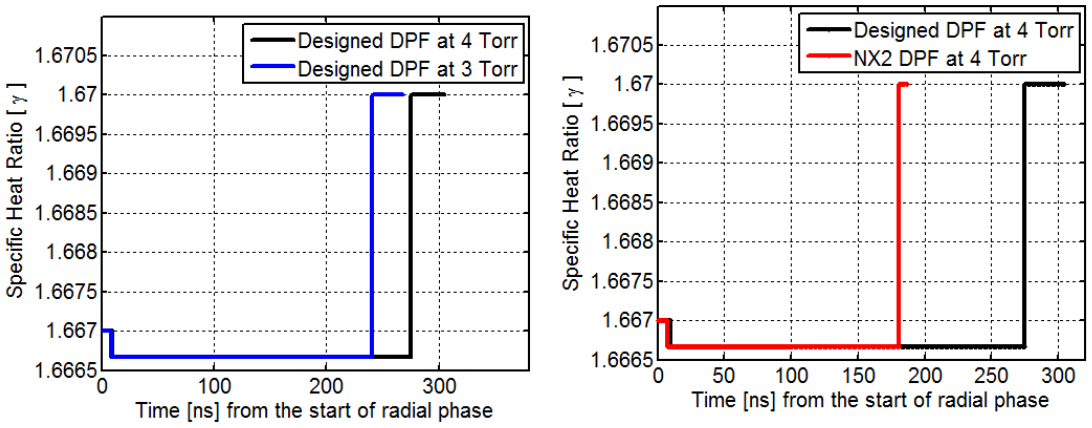

(a) (b)

Fig.(4-21): (a) Specific heat ratio γ vs. time for the designed DPF at 4 Torr and 3 Torr. (b) Specific heat ratio γ vs. time for the designed DPF and NX2 DPF at 4 Torr.

Fig.(4-21a) shows specific heat ratio γ vs. time for the designed DPF at a pressure 4 Torr and 3 Torr. The ionization and excitation processes play an important role in the energy balance in the plasma gas. This effect can be described by the effective specific heat ratio γ. It is known that the radius ratio of a plasma pinch depends on the specific heat ratio γ of the pinch plasma, where radius pinch ratio is defined as: radius of plasma pinch column/radius of anode. If specific heat ratio γ is reduced the radius ratio becomes reduced. This reduction in radius ratio means an increase in plasma density. When the specific heat ratio is at $\gamma = 1.667$, this is case of the typical situation of a deuterium plasma focus pinch. We expect such a large increase in pinch density to affect the neutron yield whilst the change in temperature has little effect because the thermonuclear component is insignificant compared with the beam-gas target component in the range of operation of all present plasma focus devices [111]. The specific heat ratio decrease with

increasing gas pressure, while the specific heat ratio with higher pressure.

Fig.(4-21b) shows that the variation of specific heat ratio γ . The specific heat ratio increases with the increase in gas pressure until the steady at 1.67 for both the designed and NX2 DPF.

4.24: The Charge Number vs. Time

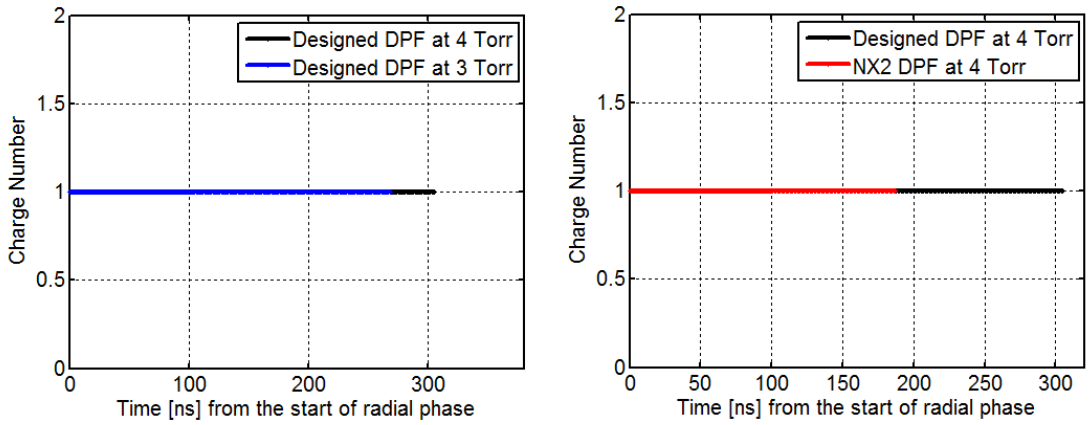

(a) (b)

Fig.(22): (a) Charge number vs. time for the designed DPF at 4 Torr and 3 Torr. (b) Charge number vs. time for the designed DPF and NX2 DPF at 4 Torr.

Fig.(4-22a) shows the variation of the charge number with the time from the start of radial phase at the pressure 3 Torr and 4 Torr. The charge number at both pressures has fundamentally the same character. The straight lines through the origin for the curve indicate that both the charge number at pressure 4 Torr and the Charge number at pressure 3 Torr are independent of T. It is clear that duration of the pinch increases as pressure increased.

Similar behavior is detected of charge number vs. time as figure (4-22b) for the designed DPF and the standard DPF. It is clear that the value of charge number does not change from the value of unity for both DPF.

4.25: The Plasma Self – Absorption Correction Factor vs. Time

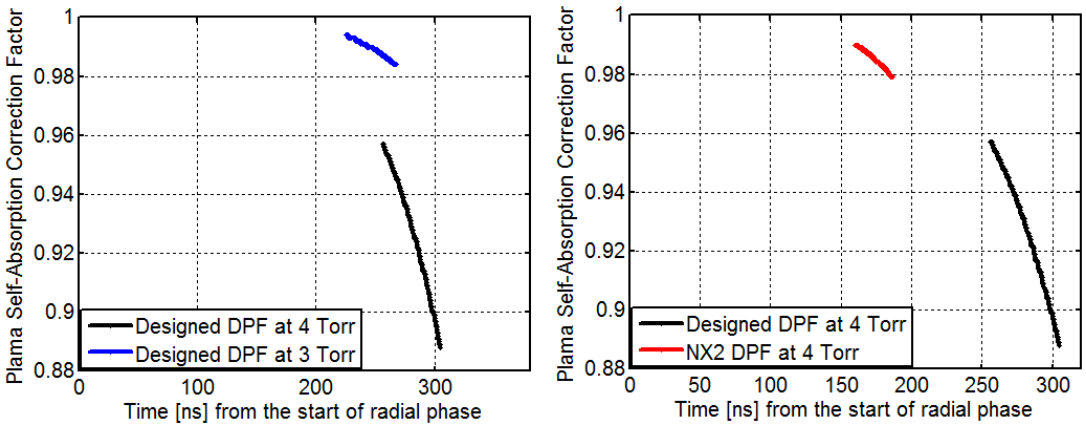

Fig (4-23): (a) Plasma self – absorption correction factor vs. time for the designed DPF at 4 Torr and 3 Torr. (b) Plasma self – absorption correction factor vs. time for the designed DPF and NX2 DPF at 4 Torr.

Fig.(4-23a) shows the Plasma self – absorption correction factor as a function to time from the start of radial phase at two different pressures. It is clear that plasma self – absorption correction factor reduces the pinch duration as pressure is decreased. The self – absorption correction factor at 4 Torr lasts more time with the increase of the pressure.

Fig.(4-23b) indicates that there is good agreement between designed DPF and NX2 DPF at 4 Torr. Nonetheless, the designed DPF starts at later time than the NX2 DPF and last more time than the standard DPF.

4.26: The Radial Phase Piston Work in % of E_0 vs. Time

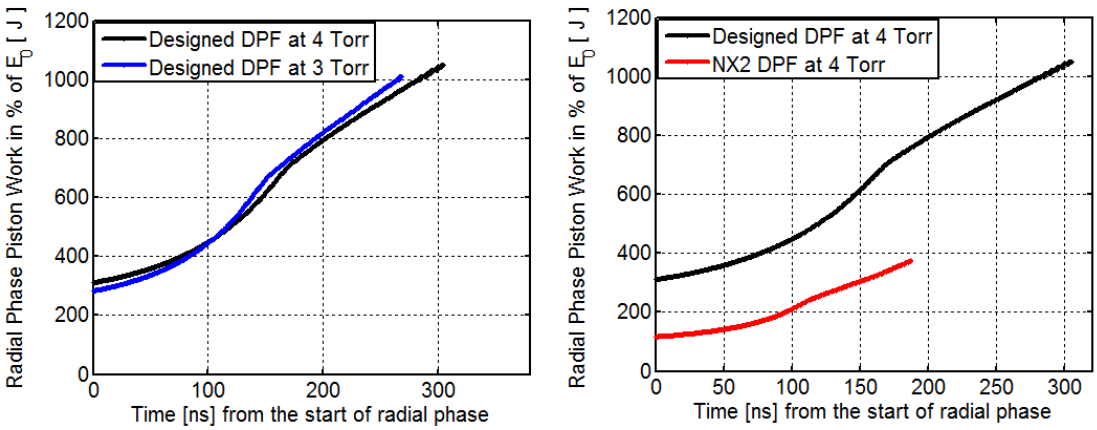

Fig.(4-24): (a) Radial phase piston work in % of E_0 vs. time for the designed DPF at 4 Torr and 3 Torr. (b) Radial phase piston work in % of E_0vs. time for the designed DPF and NX2 DPF at 4 Torr.

Fig.(4-24a) shows the piston work which is the main path to transfer energy into the plasma focus tube. The radial EINP computes the cumulative work done by the current sheath in the radial phases or the work done by the dynamic resistance during radial phase expressed as % ofE_0 [99].The piston work deposited in the plasma increases steadily at the end of the axial phase and then rises sharply and up to more 1050 J at 4 Torr and up 1010 J at 3 Torr in the radial phase. It was seen from the radial phase piston work in % of E_0 that it increased with the increase in filling gas pressure.

Fig.(4-24b) shows a comparison of theoretical calculations between the designed DPF and NX2 DPF at 4 Torr. It is noted that the radial phase piston work in % E_0 of is related to the pressure. The radial phase piston work in % of E_0 is 1050 J for designed DPF, 374 J for NX DPF.

4.27: The Soft X – Ray Radiation Energy Emission vs. Time

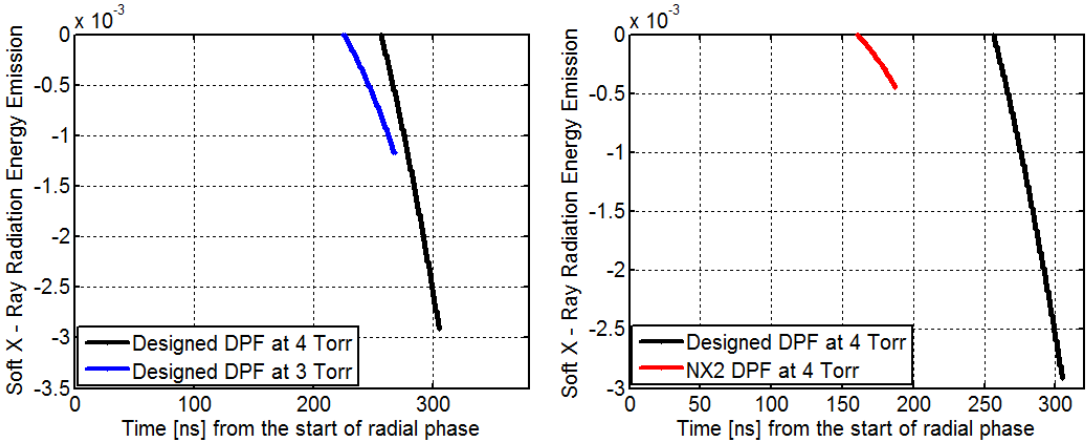

Fig.(4-25): (a) Soft X – ray radiation energy emission vs. time for the designed DPF at 4 Torr and 3 Torr. (b) Soft X – ray radiation energy emission vs. time for the designed DPF and NX2 DPF at 4 Torr.

Fig. (4-25a) shows the soft X – ray radiation energy with time at two different pressures value. It is seen that for 4 Torr pressures, the soft X – ray radiation energy emission is higher and longer as compared to the value at 3 Torr. It was seen that the Soft X – ray radiation energy emission initially increased with the increasing in filling gas pressure and subsequently Y_{sxr} radiation energy emission decreases with lower pressures.

Fig.(4-25b) is a comparison between the designed DPF and NX2 DPF of Y_{sxr} versus time from the start of radial phase. The figure shows general agreement between them. The soft X-ray emission from the plasma focus using different gases has the drop – off of Y_{sxr} on the low – pressure side is very similar to Y_{sxr} on the high – pressure side, but the designed DPF has drop – off on the high P_0 side shows a sharper drop off compared to NX2 DPF.

4.28: Neutron Yield vs. pressure

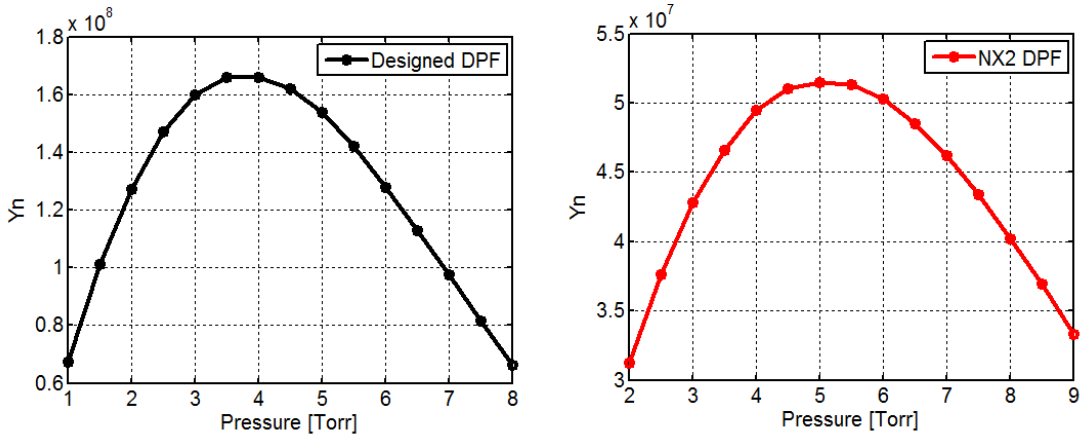

(a) (b)

Fig.(4-26): (a),(b) Neutron yield vs. pressure for the designed DPF and NX2 DPF.

Fig.(4-26): (a) and (b) show that the variations of neutron yield versus pressure in the designed DPF which is reasonably agree with standard NX2 DPF curve. As the pressure is increased the neutron yield increases to a peak point and then decreases. The neutron yield peak point (1.66×10^8 neutron per shot) of the designed DPF is at a pressure 4 torr, while the peak point of neutron yield (5.15×10^7 neutron per shot) is at a pressure 5 torr. It is clear that the designed plasma focus yields higher neutron yield than the standard one.

CHAPTER

FIVE

Conclusions and Suggestions

5.1:Conclusions

In This study a theoretical dense plasma focus has been designed depending on simple mathematical formulae. The results are implemented in Lee code to see whether it matches the well known behavior of the dense plasma focus. Representing the trace of the total tube current with time graphically, give a hint that the machine should work properly. Therefore, the other main parameters relevant to the plasma dynamics and achievement of machine are calculated, graphically displayed and studied for two values of pressure. Further the designed machine compared to a known dense plasma focus at the same pressure. The behaviors of the entire parameters involved in this study are consonant.

1. The tube voltage verses time yields higher amplitude than the known DPF at the same pressure.
2. The axial speed vs. time of designed plasma focus agrees with standard axial speed DPF at the same pressure.
3. The behavior of axial position trajectory vs. time is consistent with the same pressure of both the designed and the standard plasma focus.
4. The radial position of shock of the designed plasma focus is higher and takes greater period of time from the standard one.
5. The pinch elongation trajectory for the designed dense plasma is longer than the standard one since it lasts more time.
6. Indeed, it is found that the designed plasma focus in complete agreement with the standard dense plasma focus machines.
7. The interest of this study is reflected the possibility of finding the best values of the physical parameters affecting the operation of

the designed dense plasma system and control the radiation emissions and neutrons yield.

8. Further undoubtedly getting the biggest output of neutrons yield is best to obtain a fusion nuclear reaction. The designed dense plasma focus in this study gives a reasonable neutrons yield compared to the known DPF.

5.2:Suggestions for future work

In conclusion, we suggest that the designed system (DPF) is to be built and carry out experimental scientific research. We will ask for some others programs in order to set up a wide researches to compare the experimental work with calculations that accomplish theoretically. By using those programs and the build designed DPF one can know the reasons for some phenomena that occur and thus these leads to possibility of development in this area.

REFERENCES

References

[1] Brand F., (2006)'' Plasma Physics,'' School of Physics, University of Sydney NSW, Notes course in Plasma Physics Australia.

[2] Paul K. Chu XinPei Lu , (2010)'' Low Temperature Plasma Technology Methods and Applications'' , CRC press, Taylor & Francis Group, (Boca Raton, London, New York).

[3] Rucker H. O. (1984),'' Introduction to Plasma Physics,'' Notes Lectures, Institute of Physics Karl – Franzens – University Graz, Austria.

[4] Morozov A. I., (2013), '' Introduction to Plasma dynamics'', CRC press, Taylor & Francis Group, (Boca Raton, London, New York).

[5] Bellan P. M., (2004), ''Fundamentals of Plasma Physics'', Pasadena, California.

[6] Chen F.F., (1984), “Introduction to Plasma Physics and Controlled Fusion”, Plenum Press, New York.

[7] Howard J. ,(2002),'' Introduction to Plasma Physics'', C17 Lecture Notes.

[8] Zionist M.W., (2006), "Introduction to Plasma Physics", Oman.

[9]Shukla N., (2012),'' Generation of Magnetic Fields in Plasmas'', Umeå, Sweden.

[10]Shihab M. A., (2013),'' The Dynamics of the Plasma Boundary Sheath'', M. Sc thesis, University of Bern in Bochum.

[11] Lieberman M. A.,(2003) ,''Introduction to Plasma Discharges and Processing'', ORIGIN OF MINI-COURSE.

[12] Lieberman M. A., Lichtenberg A. J.,(2005),'' Principles of Plasma Discharges and Materials Processing '' New Jersey, Canada.

[13] Fitzpatrick R., (1986), '' Plasma Physics'', The University of Texas at Austin.

[14] Abdulameer M R. , (2014),'' Study the plasma characteristics and CuO nanoparticles by pulsed laser deposition, M.Sc. Thesis, University of Baghdad.

[15] Krall N. A. and Trivelpiece A. W., (1973), "Principles of plasma physics" International Student Edition-International Series in Pure and Applied Physics, Tokyo McGraw-Hill.

[16] Al Agry A., (2013),''Study of a Non-Equilibrium Plasma Pinch with Application for Microwave Generation,'' M. Sc thesis, University of Nevada, Las Vegas.

[17] Goldston R. J. and Rutherford P. H., (1995),'' Introduction to Plasma Physics'', IOP Publishing .

[18] Smid T. ,(2010),'' Theoretical Principles of Plasma Physics and Atomic Physics'', M.Sc. Physics, Cambridge UK.

[19] Cahill B. J., (2012),'' An investigation of the influence of plasma parameters on the spectra of helium plasmas'', M. Sc. thesis, University College Cork.

[20] Harms A. A., (2000), “Principles of Fusion Energy: An Introduction to Fusion Energy for Students of Science and Engineering”, World Science press.

[21] Schmidt A., Tang V., Welch D., (2012), "Fully Kinetic Simulations of Dense Plasma Focus Z-Pinch Devices", Phys. Rev. Lett. V (109).

[22] Decker G., Flemming L, Kaeppeler H. J., Oppenlander T., Pross G., Schilling P., Schmidt H., Shakhatre M. and Trunk M., (1980) “current and neutron yield scaling of fast high voltage plasma focus” J.Plasma physics ,V(22),No.(33).

[23] Gerdin G. ,Stygar W., Venneri F. (1981) “Faraday Cup analysis of ion beams produced by a dense plasma focus” Journal of Applied Physics ,V(52),No.(5),pp.(3269-3275).

[24] Stygar W. , Gersin G., Venneri F., Mandreakas J., (1982) “particle beams generated by a 6-12.5 KJ dense plasma focus” J.Nuclear Fusion ,V. (22),No.(9),pp.(1161-1172).

[25] Hill R.A., Hubbs J.W.,(1983) “A multi-shot dense plasma focus with improved cathode design” J.physics Letters A, V.(98),No.(8-9),pp.(417-20).

[26] Bibao L., Bruzzone H.,(1984) “Instability of the current sheath in plasma focus devices” J.physics Letters A, V.(101), No(5-6),pp.(239-307).

[27] Boltog I., Gancin M.,Mihut L.,Zammbreanu V. and Zoita V.,(1985) “Interferometric Method for Electronic Density Measurement in a plasma Focus Device” Journal of plasma physics,V.(25), No.(3),pp.(263-275).

[28] Kato.Y, (1986) “Generation of soft x-ray using a rare gas –hydrogen plasma focus and its application to x-ray lithography”, J.Applied Physics Letter, V.(48),No.(11),pp.(686-688).

[29] Jager U., Herold H.,(1987) “Fast ion kinetics and fusion reaction mechanism in the plasma focus” J.Nuclear fusion ,V.(27),No.(3),pp.(407-423).

[30] Sadowski M., Zebrowski J., Rydygier E. and Kucinski J.,(1988) “Ion emission from plasma-focus facilities” J.Plasma Phys.control.fusion ,V.(30),No.(6),pp.(763).

[31] Zambreanu V. , Doloc C.M.,(1992) “An electro dynamical model for the ion behaviour in the final plasma focus stages ” Journal plasma phys.control.fusion, V.(34),No.(8),pp.(1433).

[32] Kato Y.,(1994) “Electrode Lifetime in a plasma Focus Soft X-Ray Source” J.Apple.Phys, V.(33), No.(8)part1, pp.(4742).

[33] Kelly H. , Marquez A.,(1995) “The influence of multiple scattering on the ion spectrum from a Thomson spectrometer in a plasma focus device” J.Measurement science and Technology ,V.(6),No(4),pp.() .

[34] Zakaullah M. , Ahmed L., Murtaza G., Beg M.M. (1997) “Influence of magnetic probe presence on current sheath dynamics in plasma focus operation ” J.Fusion Engineering and Design ,V.(36), pp.(437-446) .

[35] Aliaga-Rossel R., Choi P. (1998) “Experimental observations of the spatial anisotropy of the neutron emission in a medium energy plasma focus ” J.Plasma Science ,V.(26),No.(4),pp.(1138-1145).

[36] Woon C., Duck P.,(1999) “X-ray Radiation of the plasma Focus With Inverse Pinch Switch” Japanese Journal Of Applied Physics ,Vol.38,No.(2A),pp.(913).

[37] Gribkov V. A., Mahe .L, Lee .P , Lee S. , Srivastav A. ,(2000),'' Dense Plasma Focus radiation source for microlithography & micro-machining'', Nanyang Technological University, Singapore, V.(4226). pp.(151-159).

[38] Dubrovsky A .V., Gribkov V. A., Ivanov Y. P., Lee P., Lee S., Liu M., Samarin V . A., (2001),'' 0.2-kJ and 2-kJ high rep rate Dense Plasma foci, Nukleonika V (1), pp. (107–111).

[39]Babazadeh A.R., Roshan M.V., Habibi H., Nasiry A., Memarzadeh M.,(2002),'' X-ray and Neutron Emission Studies in a New Filippov Type Plasma Focus'', Braz. J. Phys. V.(32), No.1, pp.(89-94).

[40] Pouzo J., Acuňa H., Milanese M., and Moroso R., (2002) ,'' Relativistic electron beams detection in a dense plasma focus'', Eur. Phys. J.D, V. (21), No.(1) pp.(97-100).

[41] Randy H.P.Y., Loke S.S., Lee P., Rawat R.S., (2003) ,'' Effects of Insulator Sleeve Length on Neutron and X-ray emissions from Deuterium filled Dense Plasma Focus Device'', Fusion and Plasma Phys., V(27A), pp.(1.208).

[42] Silva P., Moreno J., Soto L., Birstein L., Mayer R. E., and Kies W., (2003) ,'' Neutron emission from a fast plasma focus of 400 Joules'', Applied Physics Letters, V (83), N (16). pp.(3269-3271).

[43] Bhuyan H., Mohanty S. R., Neog N. K., and Bujarbarua S., (2004) ,'' Comparative study of soft x-ray emission characteristics in a low energy dense plasma focus device'', Journal of Applied Physics V.(95), N(6).pp(2975-2981).

[44] Soto L., Silva P.,(2004) ,''Research on pinch plasma focus devices of hundred of kilojoules to tens of joule'' Braxilian Journal of physics, V.(34) N. (4B), pp.(1814).

[45] Yap S. L., Wong C. S., Choi1 P., Dumitrescu C. and Moo S. P., (2005) ,'' Observation of Two Phases of Neutron Emission in a Low Energy Plasma Focus'', Japanese Journal of Applied Physics V (44), N (11), pp. (8125–8132).

[46] Zhang T., Rawat R. S., Hassan S. M., Lin J. J., Mahmood S., Tan T. L., Springham S. V., Gribkov V. A., Lee P., and Lee S., (2006) ,'' Drive Parameter as a Design Consideration for Mather and Filippov Types of Plasma Focus '', IEEE Transactions on Plasma Science, V (34), N (5), pp.(2356-2362).

[47] Gribkov V. A., Banaszak A., B Bienkowska, Dubrovsky A. V., Ivanova-Stanik I., Jakubowski L., Karpinski L., Miklaszewski R. A., Paduch M, Sadowski M J, Scholz M, Szydlowski A and Tomaszewski K, (2007) ,'' Plasma dynamics in the PF-1000 device under full-scale energy storage: II. Fast electron and ion characteristics versus neutron emission parameters and gun optimization perspectives'', J. Phys. D: Appl. Phys., V(40) pp.(3592–3607).

[48] Lee S. and Saw S. H., (2008) ,'' Pinch current limitation effect in plasma focus'', Appl. Phys. Lett. V.(92), N.(2), pp. (1-3), American.

[49] Lee S., Saw S. H., Lee P. C. K., Rawat R. S., and Schmidt H., (2008),'' Computing plasma focus pinch current from total current measurement'', Appl. Phys. Lett. V.(92), N.(11), pp.(1-3). American Institute of Physics.

[50] Lee S., (2008),'' Current and neutron scaling for megajoule plasma focus machines'', Plasma Phys. Control. Fusion, N.(50), V.(10) pp. (1-14).

[51] Yap S. L., Lee S. H., Lim L. K. and Wong C S, (2008),''Dynamic Studies of a Small Plasma Focus Device'', Plasma Research Laboratory, Physics Department, Faculty of Science, University of Malaya, 50603 Kuala Lumpur, Malaysia, pp.(51-54).

[52] Lee S & Saw S H, (2008) ,''Neutron Scaling Laws from Numerical Experiments'', Journal of Fusion Energy, V.(27), No.(4), pp(292-295).

[53] Lee S, Saw S H, Soto L, Springham S V and Moo S P, (2009) ,'' Numerical experiments on plasma focus neutron yield versus pressure compared with laboratory experiments'', Plasma Phys. Control. Fusion 51 075006 pp.(11).

[54] Verma R., Rawat R.S., Lee P., Lee S., Springham S.V., Tan T.L., Krishnan M., (2009) ,'' Effect of cathode structure on neutron yield performance of a miniature plasma focus device'', Physics Letters, V.(373A) ,pp.(2568–2571).

[55] Mohammadi M A, Sobhanian S, Wong C S, Lee S, Lee P and Rawat R S, (2009) ,'' The effect of anode shape on neon soft x-ray emissions and current sheath configuration in plasma focus device'', J. Phys. D: Appl. Phys. V.(42) , pp.(10).

[56] Saw S H, Lee P C K, Rawat R S, and Lee S, (2009) ,'' Optimizing UNU/ICTP PFF Plasma Focus for Neon Soft X-ray Operation'', IEEE Transactions on Plasma Science, V (37), N.(7). pp.(1276-1282)

[57] Rafique M. S. , Lee P., Patran A. , Rawat R. S., Lee S.,(2010), '' Radiation Emission Correlated with the Evolution of Current Sheath from a Deuterium Plasma Focus'', J Fusion Energy, Singapore.

[58] Borthakur T K and Shyam A, (2010),'' Analysis of axial neutron emission pulse from a plasma focus device '', Indian Journal of Pure and Applied Physics V (48), pp.(100- 103).

[59] Zapryanov S., Yordanov V., Blagoev A., (2011), '' Measurements of the Basic Characteristics of the Dense Plasma Focus Device'', Bulg. J. Phys, V(38), pp.(184–190).

[60] Tarifeño-Saldivia A., Pavez C., Moreno J., and Soto L. , (2011) ,''Dynamics and Density Measurements in a Small Plasma Focus of Tens-of- Joules-Emitting Neutrons'', IEEE Transactions on Plasma Science, V (39), N.(2). pp.(756-760).

[61] Lee S., (2012),'' Radiation Enhancement and Applications Scaling from the UNU/ICTP PFF'', Nanyang Technological University, Singapore, pp.(1-13).

[62] Lee S, Saw S H, Rawat R S, Lee P, Talebitaher A., Abdou A E, Chong P L, Roy F, Singh A, Wong D and Devi K, (2012),'' Correlation of Measured soft x-ray pulses with modeled dynamics of the plasma focus'', IEEE Transactions on Plasma Science, pp.(1-6).

[63] Salehizadeh A. , Movahhed M. S , Zaeem A. A., Heidarnia A., Sabri R. , Mahmoudi M. B., Rahimi H., Rahimi S., Johari E., Torabi M., Damideh V., (2013),'' Preliminary Results of the 115 kJ Dense Plasma Focus Device IR-MPF-100'', J Fusion Energy 32, pp.(293–297).

[64] Afsharmanesh M. and Habibi M., (2013),'' Experimental study and analysis of multiple peaks in the SXR emitted from a 4 kJ plasma focus device'', Eur. Phys. J. D, V.(67), No.(70), pp.(1-8).

[65] Ellsworth J. L., Falabella S., Tang V., Schmidt A., Guethlein G., Hawkins S., and Rusnak B., (2014),'' Design and initial results from a kilojoule level dense plasma focus with hollow anode and cylindrically symmetric gas puff '', Rev. Sci. Instrum, V.(85), pp.(1-10).

[66] Fogliatto E., Gonz_alez J., Barbaglia M. and Clausse A., (2014),'' A model of hard X-rays emission from free expanding Plasma-Focus discharges'', Journal of Physics: Conference Series, V.(511), pp.(1-4).

[67] Alaçakır A., Öncü T., Kurt E., Recepoğlu E., Akgün Y., A. S., Bölükdemir İ. T. Ç., Karadeniz H., Elmalı A., Yeşiltaş Ö., Zararsız S., Aksu Gökhan L., K., Baykal A., Reyhancan İ., (2007) "3 kJ Plasma Focus System:

Design, Construction and Experiments", Turkish Atomic Energy Authority.

[68] Willenborg D. L., Hendrick C. D., (1976), "Design and construction of a dense plasma focus device", charged particle research laboratory, department of electrical engineering, University of Illinois, Contract No. AFOSR-74-2643, Project Task No. 9751-03.

[69]Khan M Z., Yap S L. and Wong C s., (2014),'' Estimation of electron temperature and radiation of a low energy (2.2KJ) plasma focus device'', Indian J Phys, V(88), No(1), pp.(97-102).

[70]Mather J. W.,(1965),'' Formation of a High-Density Deuterium Plasma Focus'', Phys. Fluids 8,No.(2),pp.(366).

[71] Baghdadi R., Amrollahi R., Habibi M., Etaati G. R., (2011), ''Investigation of the Neutron Angular Distribution and Neutron Yield on the APF Plasma Focus Device'', J Fusion Energy , V(30) , pp (72 -77).

[72]Tang V., Rusnak B.,(2008),'' Review of Dense Plasma Focus Technology for Intense and Directional Neutron Sources'', Lawrence Livermore National Laboratory LLNL-TR-401857.

[73] Rawat R.S.,(2012),''High Energy Density Pulsed Plasmas in Plasma Focus: Novel Plasma Processing Tool for Nanophase Hard Magnetic Material Synthesis'', Nanoscience and Nanotechnology Letters V(4), pp.(1–24).

[74] Ghanei V., Abdi M. R., Shirani B.(2014),"Design and construction of a 20- kJ filippov-type plasma focus ", American Journal of Physics and Applications, V.(2) No. (1), pp. (31-34).

[75] Varma R., Roshan M. V., Malik F., Lee P., Lee S., Springham S. V., Tan T. L., Krishnan M. and Rawat R. S. , (2008) "Compact sub – kilojoule range fast miniature plasma focus as portable neutron source", Plasma Sources Science and Technology, V.(17), No. (4) , pp (11).

[76] Soto L., (2005), "New trends and future perspectives on plasma focus Research", Plasma Phys. Control. Fusion, V (47), pp (361–381).

[77] Tafreshi M. and Saeedzadeh E., (2006), "Studies of the hard X-ray emission from the filippov type plasma focus device, dena" J. Fusion Energy V(25), N (3), pp. (207-211).

[78] Bruzzone H. and Vieytes R., (1993), "The initial phase in plasma focus devices" Plasma Phys. Controlled Fusion, V.(35), No (12), pp. (1745).

[79] Khaleel S. M., (1989), '' Scaling of Dense Plasma Focus Compartment'', M.Sc thesis submitted to the Second College of Education, University of Baghdad.

[80] Silva P., Favre M., Chuaqui H., Wyndham E., and . Choi P., (1996), "Studies of current sheath evolution in a small plasma focus device" High-Power Particle Beams, 11th International Conference on V (1), pp. (570 – 573).

[81] Rafique M. S., (2000),'' Compression dynamics and radiation emission from a deuterium plasma focus,'' Ph. D thesis, National institute of education, Nanyang Technological University, Singapore.

[82]Kashani, M. A. M.; Sato, K.; Miyamoto, T.; Baba, A.; Horiuchi, R.; Taka sugi, K.; Sasaki, S.; Lu, M.; Vikhrev, V., (2001), ''Effects of Cathode Electrode in Plasma Focus Discharges'', Academia Sinica, Taiwan, pp. (244-246).

[83]Kashani M. ,(2003),''Energy Dissipation In Run-Down Phase Of Mather-Type Plasma Focus Discharges'', J. Phys. Soc. Jpn. V(72), No.(3), pp. (526-532).

[84] J. W. Mather, (1971), Dense Plasma Focus, In Methods of Experimental Physics, Lovberg R. H. and Griems H. R., Academic Press, New York, V(9b), pp. (187-249).

[85] Scholz M., Bieńkowska B., Borowiecki M., Ivanova-Stanik I., Karpiński L., Stępniewski W., Paduch M., Tomaszewski K., Sadowski M., Szydłowski A., Kubeš P., Kravárik J. , (2006),'' Status of a mega-joule scale Plasma-Focus experiments,'' Nukleonika, V(51) , N(1), pp. (79−84).

[86] Pătran A. C. (2002) “Electron and Medium Energy X-ray Emission from a Dense Plasma Focus” PhD thesis, National Institute of Education, Nanyang Technological University, Singapore.

[87] Peratt A. l., Dessler A. J., (1988),'' Filamentation of Volcanic Plumes on the Jovian satellite IO'', Astrophysics and Space Science, V (144), pp. (451-461).

[88] Serban A., (1995),'' Anode geometry and focus characteristics, PhD thesis'' School of science, Nanyang Technological University, Singapore.

[89] Bernard A., Bruzzone H., Choi P., Chuaqui H., Gribkov V, Herrera J., Hirano K., Krejci A., Lee S., Cluo, Mezzetti F., Sadowski M., Schmidt H., Ware K., Wong C.S., Zoita V., (1998),'' Scientific status of plasma focus research,'' J. Moscow phys. V (8) , pp (93-170) .

[90] Al Agry A., (2013), "Study of a Non-Equilibrium Plasma Pinch with Application for Microwave Generation", PhD thesis, Department of Electrical and Computer Engineering, University of Nevada, Las Vegas.

[91] Mahe l., (1996), “Soft X-rays from compact plasma focus” Ph.D. thesis, School of Science, Nanyang Technological University, Singapore.

[92] Bing S., (2000), "Comparative study of dynamics and X-ray emission of several plasma focus devices" PhD thesis, Physics Division, School of Science Nanyang Technological University, Singapore.

[93] Talebitaher A., (2012),'' Coded aperture imaging of nuclear fusion in the plasma focus device'', Ph.D. thesis, School of Science, Nanyang Technological university, Singapore.

[94] Guixin Z., (1999),'' Plasma Soft X-ray Source for Microelectronic Lithography'', Ph.D. thesis, School of Science, Nanyang Technological University, Singapore.

[95] Khan M. Z., Ling Y. S., San W. C.,(2013),'' Variation of Radiation Emission with Argon Gas Pressure in UM Plasma Focus with the Hollow Anode '', Journal of Applied Sciences, V(3), pp.(194-201).

[96] Qayyum A., Hassan M., Zakaullah M., (2010) ''Nitriding and carburizing of titanium by using plasma focus radiation'', International Scientific Spring, National Centre for Physics, Islamabad. J.

[96] Ceccolini E., (2012),'' Development and performance assessment of a Plasma Focus electron beam generator for Intra-Operative Radiation Therapy'', PhD thesis, University of Bologna, Italy.

[97] Bernstein M. J., Meskan D. A., Paassen H. L., (1969), “Space, Time, and Energy Distributions of Neutrons and X Rays from a Focused Plasma Discharge” Phys. Fluids, V (12), PP.(2193).

[98] Seng L. L., (2009), Lee’s Radiative Plasma Focus Model - An Improved Implementation with Auto-tuning of Model Parameters, M.sc thesis, Nanyang Technological University, Singapore.

[99] Jassim M. K., Hady F. M., (2013),''Variation of the X-Ray Emission with Argon Gas Pressure in a UNU/ICTP PFF Plasma Focus'', Diyala Journal For Pure Sciences, Vol. (9), No. (2), pp. (38-45)

[100] Lee S., (1984), “Plasma focus model yielding trajectory and structure” in Radiations in Plasmas, B. McNamara, ed., World Scientific Publishing Co, Singapore, ISBN 9971- 966-37-9, V (2) , pp. (978–987).

[101] Lee S. and Saw S. H. (2010), A course on plasma focus numerical experiments, the Abdus Salam – International center for theoretical physics, Italy.

[102] Yap S. L., Wong C. S., Choi P., Dumitrescu C., Moo S. P., (2005),'' Observation of Two Phases of Neutron Emission in a Low Energy Plasma Focus'', Japanese Journal of Applied Physics V (44), N (11), pp. (8125–8132).

[103] Lee S., (2008),''Pinch current limitation effect in plasma focus'', Applied Physics Letters V (92), N (2), pp. (1-3).

[104] Akel M., Al-Hawat S., Lee S., (2009),''Numerical Experiments on Soft X-ray Emission Optimization of Nitrogen Plasma in 3 kJ Plasma Focus SY-1 Using Modified Lee Model'', J Fusion Energy V (28), pp. (355–363).

[105] Saw S. H., Lee S, (2011), “Scaling the Plasma Focus for Fusion Energy Considerations”, International Journal of Energy Research, V (35), pp. (81–88).

[106] Akel M., Al-Hawat S., Lee S., (2010),'' Pinch Current and Soft X-Ray Yield Limitations by Numerical Experiments on Nitrogen Plasma Focus'', J Fusion Energy, V (29), pp. (94–99).

[107] Akel M., Salo S. A., Saw S. H., Lee S., (2014),'' Properties of Ion Beams Generated by Nitrogen Plasma Focus'', J Fusion Energy, V (33), N (2), pp. (189-197).

[108] Soto L., Silva P., Moreno J., Silvester G., Zambra M., Pavez C., Altamirano L., Bruzzone H., Barbaglia M., Sidelnikov Y., Kies W., (2004), ''Research on Pinch Plasma Focus Devices of Hundred of Kilojoules to Tens of Joules'', Brazilian Journal of Physics, V (34), N (4B), pp.(1814–1821).

[109] Lee S.; Saw S.H.; Lee P.C.K.; Rawat R.S., Schmidt, H., (2008), “Computing plasma focus pinch current from total current measurement”, Applied Physics. Letters, V (92), pp. (1-3).

[110] Lee S, (2012),''Study of Plasma Focus-Enhancing Knowledge and Application Potential” Proceedings of 14 IPFS Conference, Bangkok, Thailand.

[111] Saw S. H. , Chong P. L., Rawat R. S. , Ching C. T. L., Lee P., Talebitaher A. , Lee S. , (2013),'' The Effect of Specific Heat Ratio on Neutron Yield'', IEEE transactions on plasma science, V (42), N (1), pp. (99-104).

[112] Alabraba M. A., Kamara M.A., Essi I. D., (2008), ''Energy Distribution in the Plasma Focus'', V (l.22), N (4), pp.(553-561).

[113] Saw S. H. and S. Lee, Kurt E., (2011),'' Radiative dense plasma focus computation package (RADPF) '', ISMFA - International School on Magnetohydrodynamics and Fusion Applications, Institute of Theoretical and Applied Physics, Turunc-Marmaris-TURKEY.

[114] Lee S., Saw S. H. , Hegazy H. , Ali J, Damideh V., Fatis N. , Kariri H., Khabrani A., Mahasi A., (2014), ''Some Generalized Characteristics of the Electro-dynamics of the Plasma Focus in Its Axial Phase: Illustrated by an Application to Independently Determine the Drive Current Fraction and the Mass Swept-Up Fraction'', J Fusion Energy, V.(33),No.(3) pp.(235-241).

[115] Lee S., (1998),'' Radiation Enhancement and applications scaling from the UNU/ICTP PFF'', Twelve Years of UNU/ICTP PFF- A review, The United Nations University, pp. (35- 47).

[116] Lee S., Saw S H, (2010), ''Numerical Experiments Providing New Insights into Plasma Focus Fusion Devices'', Energies, V (3),No.(4), pp. (711-737).

[117] Talaei A., Kiai S. M. S., (2009), ''Investigation of the High Pressure Regimes Effects on the Neutron Production in Plasma Focus'', J Fusion Energy V (28),No.(3), pp. (235–239).

[118] Rafique S. M., (2000),'' Compression dynamics and radiation emission from a deuterium plasma focus'', PhD. Thesis, National Institute of Education Nanyang Technological University, Singapore.

[119] Serban A., Lee S. (1998),''Experiments on speed enhanced neutron yield from a small plasma focus'', J. plasma phys., V (60), N (1), pp. (3-15).

[120] Talaei A., SadatKiai S. M., Zaeem A. A., (2010),'' Effects of admixture gas on the production of $^{18}\mathrm{F}$ radioisotope in plasma focus devices'', Applied Radiation and Isotopes, V (68) ,No.(12), pp. (2218–2222).

[121] Saw S. H., Lee S., (2011),'' The plasma focus- Numerical Experiments Leading Technology'' ,FPPT Paper PF NE Leading Technology ,pp.(1-16)

[122] Saw S. H., Lee S, (2011), “Scaling the Plasma Focus for Fusion Energy Considerations”, J. Energy Research, V (35), N (2), pp. (81–88).

[123] Saw S. H., Choon P., Lee K., Rawat R. S., Lee S., (2009),'' Optimizing UNU/ICTP PFF Plasma Focus for Neon Soft X-ray Operation'', IEEE Transactions On Plasma Science, V (37), N (7), pp. (1276-1282).

[124] Lee S., Saw S. H., (2012) “Current-Step Technique to Enhance Plasma Focus Compression and Neutron Yield”, J Fusion Energy, V (31), No.(6),pp. (603–610).

[125] Akel M., Al-Hawat S., Saw S. H., Lee S., (2010),'' Numerical Experiments on Oxygen Soft X-Ray Emissions from Low Energy Plasma Focus Using Lee Model'', J Fusion Energy, V (29), No(3), pp. (223–231).

[126] Akel M., Lee S., (2012),''Dependence of Plasma Focus Argon Soft X-Ray Yield on Storage Energy, Total and Pinch Currents'', J Fusion Energy V (31) ,No.(2) pp. (143–150).

[127] Chapman S J., (1998),'' Introduction to FORTRAN 90/95 for Scientists and Engineers'', McGraw-Hill series in general engineerig, 2nd edition.

[128] Lee S., Saw S. H., Ali J., (2013),''Numerical Experiments on Radiative Cooling and Collapse in Plasma Focus Operated in Krypton'', J Fusion Energy V (32),No.(1), pp. (42–49).

[129] Lee S., (2008), “Theoretical Basis: Plasma Focus Model (Radiative)-S Lee Model”, http://www.intimal.edu.my/school/fas/UFLF/

[130] Lee S., (1998),'' Radiation Enhancement and applications scaling from the UNU/ICTP PFF'', Twelve Years of UNU/ICTP PFF- A review, The United Nations University, pp. (35- 47)

[131] Lee S., Serban A., (1996), “Dimension and lifetime of plasma focus pinch” , IEEE Transactions on Plasma Science, V (24), No. (3), pp. (1101–1105).

[132] Bogolyubov E. P., Bochkov V. D., Veretennikov V. A., Vekhoreva L. T., Gribkov V. A., Dubrovskii A. V., Ivanov Yu. P., Isakov A. I., Krokhin O. N., Lee P., Lee S., Nikulin V. Ya., Serban A., Silin P. V., Feng X., Zhang G. X., (1998),'' A Powerful Soft X-ray Source for X-ray Lithography Based on Plasma Focusing '', Physica Scripta. V (57), pp. (488-494).

[133] Akel M., Al-Hawat Sh., Lee S., (2011),''Neon Soft X-Ray Yield Optimization from PF-SY1 Plasma Focus Device,'' J Fusion Energy V (30),No.(1) pp.(39–47).

[134] Akel M., Lee S., (2012), “Dependence of Plasma Focus Argon Soft X-Ray Yield on Storage Energy, Total and Pinch Currents'', J Fusion Energy V (31),No.(2), pp.(143–150).

[135] Lee S., Lee P., Zhang G., Feng X., Gribkov V. A., Liu M., Serban A., Wong T. K. S., (1998),'' High rep rate high performance plasma focus as a powerful radiation source'', IEEE Trans. Plasma Sci., V (26), N (4) pp.(1119–1126).

[136] Roshan M. V. and Darian M. M, (2003),'' Experimental Study of Plasma Materials’ Interaction in Plasma Focus Dena'', Journal of Fusion Energy, Vol. (22), N (1), pp. (79-82).

[137] Lee S., Lee P., Saw S. H., Rawat R. S., (2008) ,'' Numerical Experiments on Plasma Focus Pinch Current Limitation'', Plasma Phys. Control. Fusion, V (50),No.(6), pp. (1-8)

[138]Frignani M., (2007),''Simulation of Gas Breakdown and Plasma Dynamics in Plasma Focus Devices'', Alma Mater Studiorum Università Degli Studi Di Bologna.

[139] Robbins A H. , Miller W C. , Miller, Robbins, (2003),'' Circuit Analysis with Devices: Theory and Practice'', 1nd edition ,pp.(1280).

[140] Ceccolini E., (2012),'' Development and performance assessment of a Plasma Focus electron beam generator for Intra-Operative Radiation Therapy'', University of Bologna.

[141] Poškus A.,(2012),'' Energy loss of alpha particles in gases'', Laboratory of Applied Nuclear Physics, Vilnius University, pp.(1-20).

ألخلاصه

في هذا البحث تم تصميم جهاز بؤرة البلازما الكثيفة نظريا بالاعتماد على موديل (لـــي) بناءا المعادلات الرياضية لنموذج لي لكل من هندسة القطبين وعناصر الدائرة الخارجية التي تضم متسعة ومحاثة ومقاومة (RLC). وبعد اجراء الحسابات اللازمة تم إدخال نتائج التصميم في برنامج لرؤية مدى أمكانية تشغيله نظريا من خلال دراسة المعلمات المختلفة التي يوفرها البرنامج وبالتالي التعرف على ظروف تشغيله والعوامل المؤثرة عليه.

لقد اختير غار الديترويوم كغاز عامل في هذه المنظومة للحصول على ناتج نيتروني من اجل التفاعل النووي الأندماجي. وتم اختبار ودراسة المنظومة عند ضغطين مختلفين (3و4 تور) حيث درست مختلف معلماتها التي يوفرها البرنامج ونوقشت وقورنت النتائج بالاشكال البيانية. أضافة لذلك تمت مقارنة المنظومة المصممة مع منظومة قياسية تناظرها من حيث التركيب النظري وهي منظومة NX2 التي بنيت اساسا للحصول على الاشعة السينية باستعمال غازات النبيلة. اختير في البحث ان يكون غاز الديتريوم هو الغاز العامل للحصول على ناتج نيتروني من اجل المقارنة، حيث درست جميع معلمات التشغيل للمنظومة المصممة مع القياسية بالرسوم البيانية.

لقد وجد من خلال انجاز الحسابات اللازمة بأن الشكل البياني لانحدار تيار الانبوب الكلي (dip) مباشرة بعد قمة التيار مع الزمن للمنظومة المصممة متفق تماما مع الشكل العام المميز لمنظومات بؤرة البلازما التجريبية دلالة على ان حسابات التصميم صالحة لهذه المنظومة وبالتالي يمكن اجراء الحسابات. أن تصرف فولتية الانبوب مع الزمن للمنظومة المصصمة كان بنفس الشاكله مع المنظومة القياسية. وينطبق هذا على سلوك المعلمات الآخرى بين المنظومتين مثل السرعة والمسار المحوريان والمسار الى الداخل للصدمة الشعاعية ومسار وسرعة استطالة القَرْصْ ومسار وسرعة الصدمة المنعكسة شعاعيا وغيرها.

تم دراسة ومقارنة تغيرات درجة حرارة البلازما مع الزمن للمنظومتين عند نفس الضغط ولضغطان مختلفان للمنظومة المصممة وكان تصرف ماكنتا بؤرة البلازما بنفس الطريقة. وتم حساب الخسائر المتولدة من الماكنتان مثل خسائر جول و برمنشتهالنك واعادة الاتحاد وخسائر الطاقة الشعاع الخطي مع الزمن.

اخيرا وجد ان المنظومة المصممة (1.66×10^{8} neutron per shot) توفر ناتج نيتروني اكبر من المنظومة القياسية (5.15×10^{7} neutron per shot) . لقد تصرفت المنظومة

المصممة مثل المنظومة القياسية لكن كان الاختلاف في سلوك المنظومة المصممة والقياسية هو اختلاف الترتيب الهندسي للمنظومتين من حيث هندسة الاقطاب واختلاف قيم العناصر الكهربائية للدائرة الخارجية. ان المنظومة المصممة نظريا في هذا البحث يمكن ان تكون مشروع لبناء ماكنة بؤرة بلازما تطبيقية للحصول على ناتجها النيتروني العالي للاستفادة منه في اجراء تفاعل الاندماج النووي.

جمهورية العراق
وزارة التعليم العالي والبحث العلمي
جامعة بغداد
كلية التربية للعلوم الصرفة / ابن الهيثم

الدراسه النظريه لتصميم ماكنه بؤره البلازما وتحقيق العوامل المختلفه التي تؤثر على حصيله النيترون المنبعث

رسالة مقدمة إلى
كلية التربية / ابن الهيثم للعلوم الصرفة، جامعة بغداد
وهي جزء من متطلبات نيل درجة ماجستير علوم في الفيزياء

تقدم بها الطالبة
رنا عيسى بك مراد
بإشراف
أ.م.د. مصطفى كامل جاسم
أ.م.د. رعد حميد مجيد

1435هـ 2014 م